



1 **LA-ICP-MS U-Pb carbonate geochronology: strategies, progress, and**
2 **application to fracture-fill calcite**

3

4 Nick M W Roberts¹, Kerstin Drost², Matthew S A Horstwood¹, Daniel J Condon¹, , David
5 Chew², Henrik Drake³, Antoni E Milodowski⁴, Noah M McLean⁵, Andrew J Smye⁶, Richard J
6 Walker⁷, Richard Haslam⁴, Keith Hodson⁸, Jonathan Imber⁹, Nicolas Beaudoin¹⁰

7

8 ¹Geochronology and Tracers Facility, British Geological Survey, Environmental Science
9 Centre, Nottingham, NG12 5GG, UK

10 ²Department of Geology, Trinity College Dublin, Dublin 2, Ireland

11 ³Department of Biology and Environmental Science, Linnaeus University, 39231 Kalmar,
12 Sweden

13 ⁴British Geological Survey, Environmental Science Centre, Nottingham, NG12 5GG, UK

14 ⁵Department of Geology, University of Kansas, Lawrence, KS 66045, USA

15 ⁶Department of Geosciences, Pennsylvania State University, University Park, PA 16802,
16 USA

17 ⁷School of Geography, Geology, and the Environment, University of Leicester, Leicester,
18 LE1 7RH, UK

19 ⁸Department of Earth and Space Sciences, University of Washington, Seattle, WA 98195,
20 USA

21 ⁹Department of Earth Sciences, Durham University, Science Labs, Durham, UK

22 ¹⁰Laboratoire des Fluides Complexes et leurs Réservoirs-IPRA, E2SUPPA, Total, CNRS,
23 Université de Pau et des Pays de l'Adour, UMR5150, Pau, France

24

25

26

27

28

29

30

31

32

33



34 **Abstract**

35 Laser Ablation Inductively Coupled Plasma Mass Spectrometry (LA-ICP-MS) U-Pb
36 geochronology of carbonate minerals, calcite in particular, is rapidly gaining popularity as
37 an absolute dating method. The technique has proven useful for dating fracture-fill calcite,
38 which provides a powerful record of palaeohydrology, and within certain constraints, can be
39 used to bracket the timing of brittle fracture and fault development. The high spatial
40 resolution of LA-ICP-MS U-Pb carbonate geochronology is beneficial over traditional
41 Isotope Dilution methods, particularly for diagenetic and hydrothermal calcite, because
42 uranium and lead are heterogeneously distributed on the sub-mm scale. At the same time,
43 this can provide limitations to the method, as locating zones of radiogenic lead can be time-
44 consuming and ‘hit or miss’. Here, we present strategies for dating carbonates with in situ
45 techniques, through imaging and petrographic techniques to data interpretation; we focus
46 on examples of fracture-filling calcite, but most of our discussion is relevant to all carbonate
47 applications. We demonstrate these strategies through a series of case studies. We review
48 several limitations to the method, including open system behaviour, variable initial lead
49 compositions, and U-daughter disequilibrium. We also discuss two approaches to data
50 collection: traditional spot analyses guided by petrographic and elemental imaging, and
51 image-based dating that utilises LA-ICP-MS elemental and isotopic map data.

52

53

54 **1. Introduction**

55 Calcite (CaCO_3), along with other carbonate minerals (e.g. aragonite, dolomite, magnesite),
56 forms in a wide variety of geological environments as both a primary and secondary mineral
57 phase, including diagenetic, biogenic, igneous, metamorphic and hydrothermal
58 environments. Calcite can incorporate uranium upon its formation, making it a potentially
59 suitable chronometer for U-Pb and U-Th geochronology. Calcite geochronology therefore
60 has the potential to provide direct timing constraints to a broad suite of geoscience
61 applications. Calcite has been dated in the past by chemical dissolution and isotope dilution
62 (ID) with measurement by either Thermal Ionisation Mass Spectrometry (TIMS) or
63 Inductively Coupled Plasma Mass Spectrometry (ICP-MS) (e.g. Smith and Farquhar, 1989;
64 DeWolf and Halliday, 1991; Brannon et al., 1996; Rasbury et al., 1997; Richards et al.,
65 1998; Woodhead et al., 2006; Pickering et al., 2010), collectively referred to here simply as
66 Isotope Dilution (ID). More recently, there has been a proliferation in the use of laser



67 ablation (LA-) ICP-MS applied to calcite geochronology (Li et al., 2014; Coogan et al., 2016;
68 Roberts & Walker, 2016, Ring & Gerdes, 2016; Methner et al., 2016; Goodfellow et al.,
69 2017; Burisch et al., 2017, 2018; Drake et al., 2017; Hansman et al., 2017; Hellwig et al.,
70 2018; Godeau et al., 2017; Beaudoin et al., 2018; Drost et al., 2018; Mangenot et al., 2018;
71 Nuriel et al., 2017, 2019; Parrish et al., 2018; Walter et al., 2018; Smeraglia et al., 2019;
72 Holdsworth et al., 2019; MacDonald et al., 2019; Scardia et al., 2019). Presently, we are not
73 aware of successful secondary ion mass spectrometry (SIMS) U-Pb dating of carbonate
74 mineralisation, but this presents an alternative microbeam method to LA-ICP-MS.

75

76 The first review of the possibilities for carbonate geochronology was published by Jahn &
77 Cuvellier (1984), and this was substantially updated by Rasbury & Cole (2009). The latter
78 provided up-to-date discussion on U-Pb isotope systematics in carbonates, particularly
79 regarding Pb-Pb and U-Pb isochron methods, as well as a review of the applications to
80 date. At that time, both marine- (e.g. limestone, dolomite) and meteoric-water sourced
81 carbonates (e.g. speleothems and tufas) had received the most attention, due to their often-
82 favourable uranium contents, and studies of hydrothermal carbonate were scarce (e.g.
83 Brannon et al., 1996; Grandia et al., 2000). U-Pb dating of speleothems has been further
84 reviewed by Woodhead et al. (2006 and 2012), again, focussing on data generated by ID.

85

86 Now that microbeam (i.e. LA-ICP-MS and SIMS) U-Pb geochronology is proving to be a
87 useful method for a range of geoscience applications, it is pertinent to address what can be
88 achieved with the method, what the current limitations are, and where improvements can be
89 made in the future. We refer to LA-ICP-MS through the rest of this paper, but acknowledge
90 that nearly all of the points we cover are equally relevant to SIMS methods. The key benefit
91 to LA-ICP-MS dating is that its high spatial resolution can be used to relate U-Pb and other
92 geochemical analyses to imaged textures. This is critical for providing context to the
93 obtained dates. Carbonate materials are heterogeneous in composition elementally,
94 isotopically, and texturally. These factors can all lead to scatter in U-Pb data, and will often
95 hinder the ability to generate high precision (i.e. $<1\% 2\sigma$) U-Pb dates. In fact, after
96 propagation of all relevant uncertainties, final U-Pb dates typically exceed 3% precision
97 (2σ). For this reason, LA-ICP-MS carbonate U-Pb geochronology is particularly suited for
98 applications in tectonics and crustal fluid-flow, but commonly less suited for applications in
99 stratigraphy and palaeoclimate.

100



101 Here we present a review of LA-ICP-MS U-Pb carbonate geochronology, focusing on its
102 benefits and application, with particular attention to hydrothermal and diagenetic vein-filling
103 carbonates; these can constrain the ages of mineral systems, crustal deformation and fluid-
104 flow, and represent a significant growth area for this method. Using several case studies,
105 we highlight the utility of image-guided analysis, where various imaging techniques provide
106 critical context for interpreting U-Pb data. We also provide case studies for an age-mapping
107 technique that is an alternative to traditional static spot ablation, and can be used in
108 combination with sample imagery to generate U-Pb age data. Finally, we highlight issues
109 surrounding initial lead compositions, initial disequilibrium in the U-Pb system and open-
110 system behaviour.

111

112 **2. LA vs ID strategies**

113 Geochronology by ID provides the most accurate assessment of the U-Pb age of a sample
114 using calibrated isotopic tracer solutions, but it is time-consuming and requires a clean
115 laboratory facility for sample dissolution and column chemistry. The spatial resolution of ID
116 is typically much lower than that offered by microbeam techniques, although resolution can
117 be increased by using a high precision micro-drill for direct sampling. A major limiting factor
118 is that carbonate materials typically have very low U concentrations (ca. 10 ppb to 10 ppm
119 U) compared with traditional U-bearing accessory minerals (e.g., often >100 ppm U in
120 zircon). This means that: 1) comparatively large volumes of material are needed for ID
121 analyses resulting in an 'averaging' effect and reduction of spread in U/Pb space, and 2)
122 samples with lower Pb concentrations yield higher blank/sample ratios, hindering the
123 accuracy and precision of the resulting data.

124

125 LA-ICP-MS is a much quicker technique than ID, and therefore less expensive per analysis.
126 Several samples can be run in a single day, meaning the technique is ideal for screening of
127 large sample sets to find the most suitable material. The effect of blanks is negated, and
128 very low (<100 ppb) Pb contents can be analysed. However, LA-ICPMS is generally less
129 precise analytically compared to ID approaches. Another major limitation is the need to
130 normalise to a matrix-matched reference material. This means that the uncertainty of the
131 reference material becomes a limiting uncertainty, and matrix effects between materials of
132 different composition will generate scatter and/or bias in the U-Pb dates that are difficult to
133 correct for.

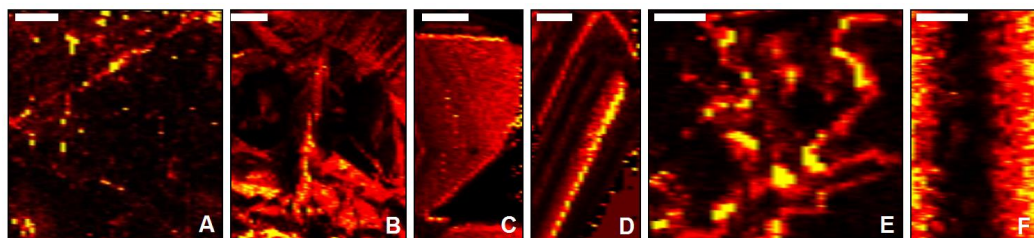


134

135 The biggest benefit of LA-ICP-MS comes from the spatial resolution (less than ca. 100 μm)
136 at which data can be obtained, particularly given the length scales of uranium concentration
137 heterogeneity in carbonate. We find that for hydrothermal and diagenetic calcite in
138 particular, uranium is heterogeneously distributed across veins and vein phases, and within
139 individual crystals (see Figure 1). Uranium concentration heterogeneity typically spans 1 to
140 3 orders of magnitude, with the length-scale of this variation being commonly much less
141 than 1 mm. Targeting of high U domains is therefore difficult without a high spatial-
142 resolution sampling method. Intracrystalline uranium distributions within calcite define
143 several patterns (see Figure 1): concentrated along cleavage planes (A), growth-zone
144 controlled (C, D and F), concentrated towards grain rims (areas of B and E), and with
145 apparent disorder (areas of B and E). Laser ablation has the spatial resolution capable of
146 targeting such elemental (and isotopic) zonation, making it easier to avoid distinguishable
147 alteration zones and inclusions at the 10-100 μm scale.

148

149



150

151 *Figure 1. Maps of uranium in vein-filling calcite from a range of geological*
152 *settings showing varying styles of distribution, see text for explanation (brighter*
153 *= higher concentration). Maps were generated using LA-ICP-MS trace element*
154 *analyses and the Lolite data reduction software. Scale bar is 1 mm.*

155

156

157 For minerals such as zircon, U-Pb ID-TIMS is considered the gold standard of
158 geochronological techniques (Renne et al., 1998). It offers significantly greater accuracy
159 than microbeam techniques by virtue of the use of gravimetrically quantified isotopic spikes,
160 and generally higher detection efficiencies. ID-TIMS does, however, consume greater
161 amounts of material. With ID methods, ages are calculated by absolute determination of the



162 number of atoms of each isotope in the sample material. In contrast, microbeam techniques
163 are relative methods, using ratio normalisation against reference minerals of known
164 composition (generally determined by ID methods).

165

166

167 For common-lead bearing minerals such as calcite, the extreme range in parent/daughter
168 ratios encountered (quoted here as ^{238}U divided by initial lead as ^{204}Pb ; a ratio known as μ),
169 means that ID does not always lead to an improvement in precision on the regressed age.

170 This is demonstrated by the schematic model in Figure 2. Sampling for ID provides an
171 average of elemental and isotopic zonation within the analytical volume, perhaps $>1\text{ mm}^3$,

172 depending on the concentration of U and Pb within the crystal(s). The resulting data should
173 be precise (depending on the sample/blank ratios), but may potentially have a small spread

174 in parent/daughter ratios (i.e. $^{238}\text{U}/^{206}\text{Pb}$) due to the averaging effect during sampling. In

175 contrast, LA sampling has the potential to target and utilise such zonation, better resolving
176 end-member μ compositions, and resulting in analyses with a greater spread in $^{238}\text{U}/^{206}\text{Pb}$

177 ratios. This potentially improves the resolving power of a regression of the measured

178 isotopic ratios allowing definition of, ideally, the high- μ (radiogenic lead) and low- μ (initial
179 lead) end-member compositions of the data array (see Figure 2). Along with the generally

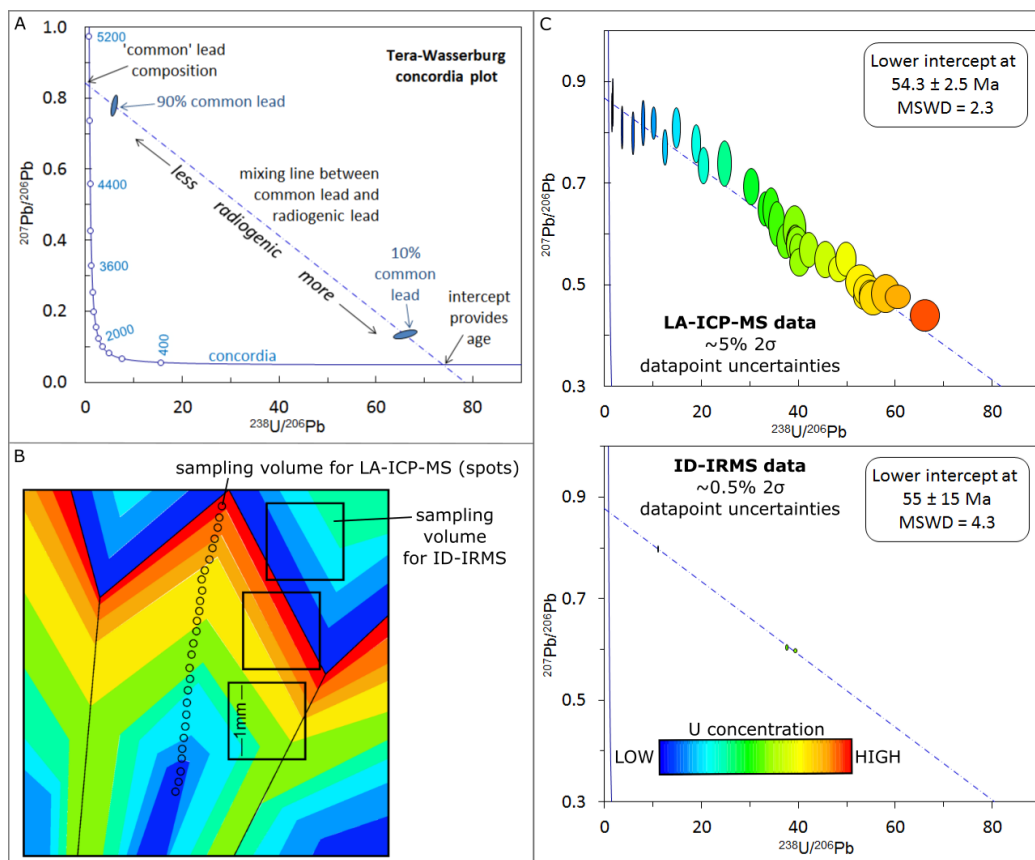
180 high- n datasets generated by the LA-ICP-MS approach, these well-constrained regressions
181 can result in similar or even greater precision age determinations than those using ID data

182 alone. However, a caveat to this, is that lower precision data points can mask true

183 geological heterogeneity.

184

185



186
187

188 *Figure 2. A) Example Tera-Wasserburg Concordia plot demonstrating the*
189 *functionality of this plot for common-lead bearing U-Pb data. B) Schematic*
190 *model of a calcite crystal with uranium zonation indicated by the colour-scale.*
191 *Typical relative sample size for ID shown by the black squares, and LA-ICP-MS*
192 *by the circles. C) Resultant U-Pb data in Tera-Wasserburg concordia assuming*
193 *constant Pb concentration across the sample, and varying U concentration, for*
194 *LA-ICP-MS sampling and analyses versus 'bulk' sampling and ID analyses, as*
195 *represented by the sampling in B. The uncertainty on the datapoints is 4-6%*
196 *(2s) for LA-ICP-MS and ~0.5-0.7% for ID.*

197
198



199 When calculating an age and uncertainty from a regression/isochron, it is assumed 1) the
200 dataset describes a single age population whose variability or scatter is derived solely from
201 the analytical process, 2) each analysis represents a closed system, and 3) all analyses
202 share the same initial Pb isotope composition. When these assumptions are satisfied, the
203 MSWD should be about 1 (Mean Squared Weighted Deviation; Wendt and Carl, 1991). LA-
204 ICP-MS data-points generally have a lower precision than those derived by ID. These lower
205 precision data-points can mask scatter that exists within the level of the data-point
206 uncertainties. This caveat must be considered when interpreting regressed data (or
207 weighted means).

208

209 In other words, age interpretations rely on isochron assumptions that can only be resolved
210 at the level of the data-point uncertainties. More precise ID data, therefore, have better
211 resolution of scatter and better constrain the likelihood that a sample does not comprise a
212 single population. However, sampling for ID can also contribute to this scatter by analysing
213 larger amounts of material, with a greater chance of including altered zones or zones from
214 different generations. A combination of ID and image-guided LA methods can therefore
215 better elucidate the likely variability in any particular sample. For applications where the
216 best possible precision is needed (e.g. for stratigraphic constraints or characterisation of
217 potential U-Pb carbonate reference materials), a workflow involving both LA-ICP-MS dating
218 followed by ID on the most favourable material is the most effective. For applications where
219 the required precision is on the order of several percent, image-guided LA-ICP-MS without
220 ID is suitable.

221 **3.**

222 **4. Identifying suitable carbonate material for dating**

223 4.1. μ ($^{238}\text{U}/^{204}\text{Pb}$) in carbonate

224 An 'ideal' U-Pb chronometer requires incorporation of U (the parent isotopes ^{238}U and ^{235}U
225 which decay to ^{206}Pb and ^{207}Pb respectively), and zero or low concentrations of initial (or
226 'common') Pb during its formation; this is typically expressed as the ratio of parent uranium
227 to initial Pb - $^{238}\text{U}/^{204}\text{Pb}$, or μ . In addition, both the parent and daughter isotopes ideally
228 remain a closed system from formation until present-day. Many chronometers lack these
229 ideal criteria but still provide successful materials for dating: the subset of 'common-lead
230 bearing chronometers' comprise small to large initial lead concentrations that are of uniform
231 composition (e.g. titanite, apatite). The ideal criteria are generally rare in carbonates, but

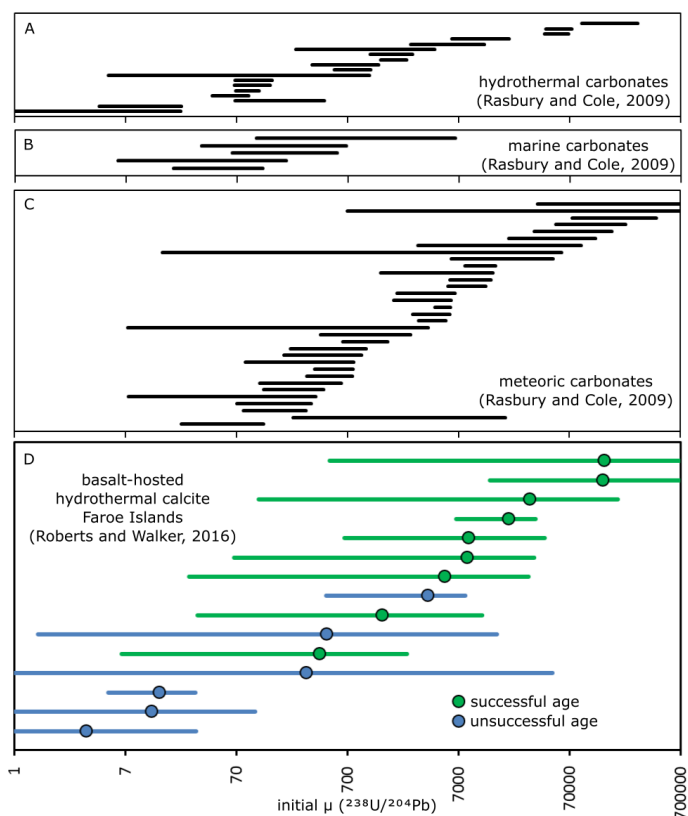


232 many carbonate materials from a range of different geological environments are successful
233 common-lead bearing chronometers.

234

235 Rasbury and Cole (2009) showed that carbonates of meteoric origin have the highest μ
236 values, and hydrothermal varieties the lowest, with marine varieties in the middle (Figure.
237 3A-C). However, the recent literature on calcite dating demonstrates that with careful
238 characterisation and sampling, high μ domains can be found in a range of hydrothermal
239 and diagenetic calcite. As an example, we plot the range of μ values recorded in very low-U
240 (<200 ppb) and low-Pb (<20 ppb) calcite taken from basalt-hosted fractures in the Faroe
241 Islands (Figure. 3D). The range of mean μ values across the fifteen samples is very large
242 (ca. 100 to 100,000), and the range within each sample is also commonly two to four orders
243 of magnitude. Of the samples providing successful U-Pb isochron ages (Roberts & Walker,
244 2016), μ values extend to as low as ~2000.

245



246



247 *Figure 3. A-C) Compilation of μ ($^{238}\text{U}/^{204}\text{Pb}$) values taken from Rasbury & Cole (2009).*
248 *Each bar is the range exhibited by an individual sample. These data were acquired using*
249 *sampling by physical separation, i.e. a dental drill. D) Compilation of μ values from basalt-*
250 *hosted vein-filling calcite in the Faroe Islands to highlight the range within crystals and*
251 *across a single region; each datapoint represents the median, and the bar represents the*
252 *range. These data represent laser ablation sampling.*

253

254

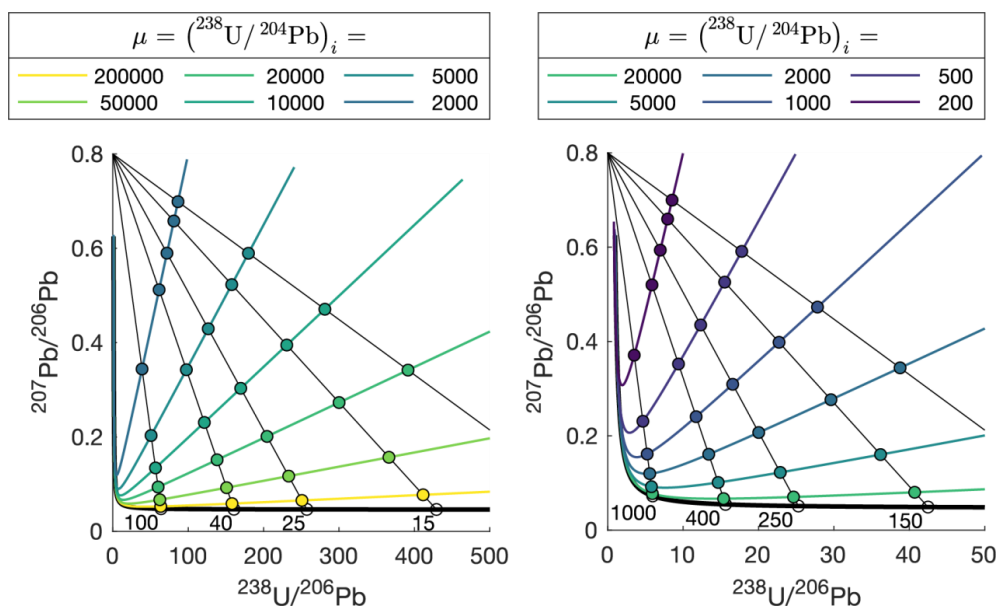
255 The amount of U needed to generate an age is dependent on two factors: (1) the age of the
256 material and (2) the initial μ ratio of the material. The younger a sample is, the less time
257 there is for the growth of radiogenic daughter Pb from parent U. With a higher μ , the ratio of
258 measured radiogenic Pb to common (initial) Pb will be higher, giving greater confidence and
259 (in general) precision and accuracy to the resulting age determination.

260

261 The effect of these factors is shown in Figure 4. Two Tera-Wasserburg plots are shown,
262 with isochrons for samples of different ages (100 to 10 Ma on the left, 1000 to 100 Ma on
263 the right). The most accurate and precise age determinations, i.e. those that can be
264 interpreted with most confidence, are generated when the sample comprises abundant
265 radiogenic lead, i.e. gets close to the lower part of the concordia curve where the
266 regression intercepts. Each plot shows regressions for individual samples between a
267 common-lead composition (~ 0.8) and a radiogenic end-member (with the age labelled). The
268 colour-coded points along each regression reflect the amount of radiogenic lead that will be
269 created by decay of ^{238}U , based upon the given μ value. For example, utilising the left plot,
270 a sample of 15 Ma, with a μ of 10,000, will have a measured $^{207}\text{Pb}/^{206}\text{Pb}$ of ~ 0.4 , equalling
271 about a 50:50 ratio between radiogenic and initial lead. To get a near concordant
272 measurement of this sample would require a μ value of over 200,000. These plots
273 demonstrate how older samples are more amenable to dating than those young in age, at
274 least when regarding the abundance of radiogenic lead. The preservation of a closed
275 isotopic system over long time periods is what makes dating old samples (i.e. Precambrian
276 materials) potentially difficult.

277

278



279
 280

281 *Figure 4. Tera-Wasserburg plots showing modelled regressions for samples of different*
 282 *age. Colour-coded spots relate to the measured isotope composition a sample would have*
 283 *at a given μ value (legend above). Ages of each regression in Ma are labelled adjacent to*
 284 *the lower intercept with concordia.*

285
 286

287 When absent of concordant analyses, both high μ and a significant spread in initial μ values
 288 are required to generate the most robust ages, as these will pin the isochron at the
 289 radiogenic end-member with greater confidence. Some calcite exhibits sufficiently high μ to
 290 generate concordant data (e.g. Richards et al., 1998; Roberts & Walker, 2016; Nuriel et al.,
 291 2017). Such robust ages are rare with a material that so commonly exhibits high initial lead
 292 abundances. Ages can be derived from isochrons with low amounts of radiogenic lead, i.e.
 293 those with low μ . Such isochrons can be regressed to provide lower intercept ages, but the
 294 confidence in these ages is subject to having well-behaved data conforming to a single
 295 population, requiring precise data-point uncertainties (e.g. Figure 5G). Such low μ
 296 isochrons can potentially give inaccurate lower intercept ages if the material is very young,
 297 and thus confirmation through multiple samples and/or alternative age constraints are
 298 favoured.

299



300 In Figure 5, we present a selection of ‘real-world’ data to highlight the potential complexity
301 of carbonate U-Pb data. These data from natural samples broadly range from undesirable
302 to most desirable from A to I, with the following notable characteristics:

303 A) Dominated by common lead with large data-point uncertainties (due to low count-rates)
304 that hamper the distinction between open-system behaviour and radiogenic ingrowth of
305 lead.

306 B) All analyses are ca. 100% common lead, with high count-rates providing a precise
307 measurement of the composition of this common lead.

308 C) Mixed and scattered data that do not fall on a single linear isochron. This is likely caused
309 by open system behaviour, potentially involving both addition and subtraction of parent
310 ^{238}U .

311 D) Majority of data define a linear array with a large spread in U/Pb ratios. Some other
312 analyses fall on a horizontal array, suggesting they experienced open-system behaviour
313 (e.g., local ^{238}U mobility).

314 E) Data form an apparent single linear array, but large uncertainties (due to low count-
315 rates) may obscure mixed ages or minor open-system behaviour.

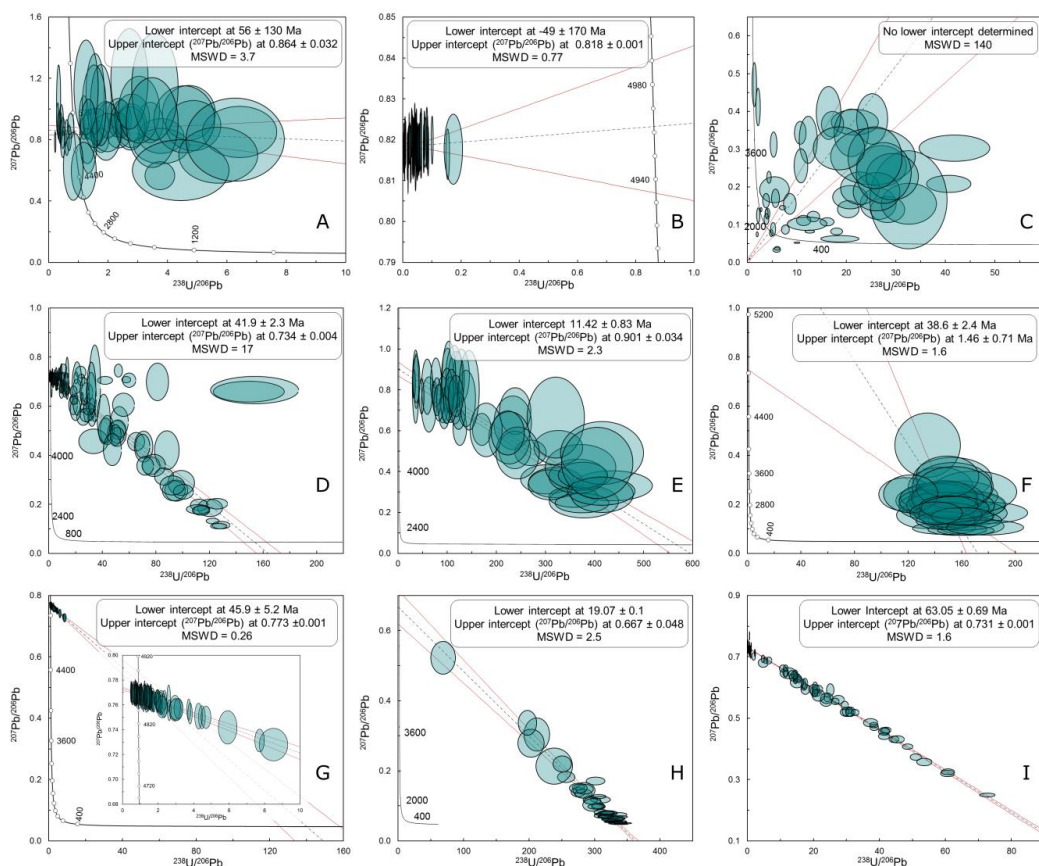
316 F) Dominated by relatively radiogenic isotopic compositions, but with large data point
317 uncertainties due to low count-rates. The narrow range in μ leads to a large age uncertainty
318 from extrapolating to the lower concordia intercept. The age uncertainty would be improved
319 with a common lead composition estimated from contemporaneous low- μ samples of the
320 same suite.

321 G) A ‘small scale isochron’ (see Ring & Gerdes, 2016). There are no radiogenic isotopic
322 compositions to anchor the extrapolation to a lower intercept concordia date, but a tight
323 data array yields a realistic intercept age.

324 H) Dominated by radiogenic isotopic compositions, and the spread in the array provides a
325 precise lower intercept date; small data-point uncertainties improve ability to identify
326 potential outliers.

327 I) A precise regression due to well-behaved closed system behaviour, high count rates
328 giving small uncertainties, and a large spread in U/Pb ratios providing a precise estimate of
329 both the age and the common lead isotopic composition.

330



331
332
333
334
335
336
337

Figure 5. Tera-Wasserburg concordia plots of natural carbonate samples from a variety of settings, with no data rejection. Lower intercept dates are quoted without propagation of systematic uncertainties. See text for explanation.

338 4.2. U and Pb contents in carbonate

339 At present, there is a lack of predictive criteria that can be used in the field or in the
340 laboratory to screen samples prior to analysis for high μ domains. Radionuclide
341 incorporation in calcite is not well understood despite several decades of interest, primarily
342 driven by the field of nuclear waste storage and characterisation (e.g. Langmuir, 1978;
343 Milton & Brown, 1987; Sturchio et al., 1998; Reeder et al., 2000, 2001; Kelly et al., 2003;
344 Weremeichik et al., 2017; Drake et al., 2018). This is because trace element incorporation
345 in calcite does not rely on thermodynamically determined partition coefficients, but by a



346 large number of phenomenological variables, including: trace element availability, calcite
347 growth rate, temperature, pH, Eh, pCO₂ and the Ca²⁺:CO₃²⁻ ratio in solution, ionic size, and
348 U complexation. Furthermore, different trace elements can be preferentially incorporated
349 into structurally different growth steps and faces of growing calcite crystals (Paquette and
350 Reeder, 1995; Reeder, 1996).

351

352 Rasbury and Cole (2009) provided a geochronology-focused review of U and Pb in calcite,
353 and we note the following salient features: 1) Pb is both particle reactive and relatively
354 insoluble; 2) Pb is found at very low levels in most fluids (ppt-ppb), providing high Ca/Pb
355 ratios; 3) Pb can substitute for Ca in the crystal lattice, although the Pb cation is larger –
356 ionic radii of Ca²⁺ and Pb²⁺ in six-fold coordination are 114 and 133 pm, respectively; 4) U
357 exists in multiple oxidation states, and its solubility is strongly affected by Eh and pH; and 5)
358 both U(VI) and U(IV) have been found in calcite, but with the latter being interpreted as the
359 most likely and most stable form.

360

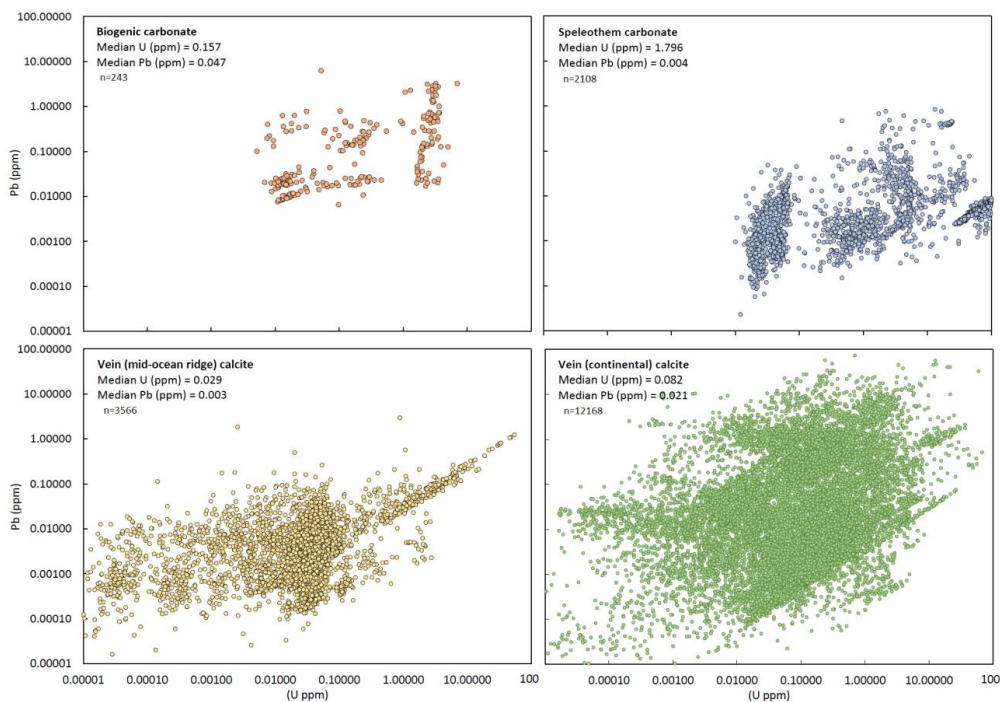
361 Points 4 and 5 above are important for understanding why and when uranium is
362 incorporated into calcite, and whether remobilisation is likely. Sturchio et al. (1998), using a
363 combination of X-ray absorption spectroscopy and X-ray microprobe fluorescence,
364 demonstrated that the uranium in a sample of spar calcite was in the form of U(IV), and that
365 U(VI) was less likely based on size and ionic structure (ionic radii of U(IV) and U(VI) in six-
366 fold coordination are 103 and 93 pm, respectively). Given that U(IV) is less mobile than
367 U(VI), this study provided important support for U-daughter geochronology. Kelly et al.
368 (2003) however, found that U(VI) as uranyl (UO₂²⁺) was the dominant species in a natural
369 sample of vein calcite, which they considered to be more representative of typical low-U
370 material than the Sturchio sample. Drake et al. (2018) found much higher concentrations of
371 uranium in calcite precipitated from deep anoxic groundwater than experimental
372 determinations that were performed in oxic conditions, and interpreted this high uranium
373 uptake as due to incorporation of U(IV) and thus that the partition coefficient for U(IV) is
374 orders of magnitude larger than for U(VI). It is evident that more data from natural
375 carbonates in different settings are needed to more fully understand the controls on U and
376 Pb incorporation.

377

378 We have compiled uranium and lead concentration data from carbonates analysed in the
379 BGS laboratory over several years (Figure 6). From our data, we see that median U/Pb_{total}



380 ratios for speleothems are ~500, whereas median values for Mid-Ocean Ridge (MOR) and
381 continental vein calcite are 8.2 and 2.6, respectively. Note that these are total Pb contents,
382 and include radiogenic Pb as well as initial Pb, which causes the short linear trends that
383 represent individual samples. Samples in Figure 6 are mostly younger than 200 Ma, or < 4
384 Ma for the speleothems. The concentration data and U/Pb ratios demonstrate that
385 speleothems in general are much more amenable to U-Pb geochronology, which is why
386 they have been the main focus for this method until the last few years. Dating vein calcite,
387 with more variable and lower contents of U, and higher contents of Pb, has a lower chance
388 of success than speleothems (although it should be noted that the speleothems in general
389 have already been visually pre-screened during sampling).
390
391



392
393 *Figure 6. Uranium and total lead contents of various carbonate materials based on a*
394 *compilation of laser ablation spot data from the British Geological Survey lab over several*
395 *years. A) Compilation of biogenic carbonates, mostly from corals; B) Speleothem*
396 *carbonates; C) Veins hosted within mid-ocean ridge oceanic crust; and D) veins hosted*



397 *within a range of lithologies from the upper continental crust, from both outcrop and*
398 *borehole samples.*

399

400

401 Ideally, a predictive framework could be constructed to aid field sampling and laboratory-
402 based sub-sampling of carbonate material for geochronological analyses. However, given
403 the large number of variables controlling U and Pb in carbonate, it is unlikely that such a
404 tool can be developed without measuring a large number of parameters in the
405 mineralising/diagenetic system. Relevant information might include the redox history of the
406 system. For example, oxidising fluids may mobilise U as U(VI), which is soluble in hydrous
407 fluids, leading to U loss during fluid-mineral interaction. Conversely, U may undergo much
408 higher precipitation into the mineral phase at redox fronts representing reducing conditions,
409 since reduced U(IV) has lower solubility. Other pertinent information for predicting success
410 includes the nature of the host rock and the source of the fluids. For example, if the
411 mineralising fluids transmit through Pb-rich units, then an undesirable enrichment in the
412 fluid Pb/Ca would take place, leading to lower initial $^{238}\text{U}/^{204}\text{Pb}$.

413

414 The complex nature of trace element uptake, including Pb and U, in carbonate
415 mineralisation is exemplified by recent studies in hydrothermal settings. Fracture
416 mineralisation in the crystalline basement of southern Sweden has been investigated
417 extensively to evaluate potential geological nuclear waste repository facilities. Several
418 studies have shown that most trace element concentrations vary over an order of
419 magnitude within calcite samples (at the thin section scale), and up to several orders of
420 magnitude across individual fractures (Drake et al., 2012, 2014; Maskenskaya et al., 2014;
421 Milodowski et al., 2018). These authors suggest that: 1) trace element chemistry does not
422 trace the source rock of the metals; 2) the co-variation of most trace elements implies
423 changing metal/Ca ratios in the fracture waters; and 3) in-situ factors affect trace element
424 incorporation, such as microbial activity, metal speciation, crystal habit, water type and co-
425 precipitation of other phases such as barite and pyrite. Our own experience of vein-filling
426 fractures matches these previous studies, as shown for example by the basalt-hosted
427 calcite in the Faroe Islands (see Figure 9).

428



429 **5. Sample screening, imaging and petrography**

430 As discussed above, it is difficult to predict which carbonate samples are most suitable for
431 U-Pb geochronology. We therefore utilise several methods to screen material, with the aim
432 of limiting the time wasted on unsuitable samples, improving the quality of data that is
433 collected, and enhancing the overall efficacy of LA-ICP-MS U-Pb carbonate geochronology.
434 The purpose of sample imaging is two-fold: it provides important spatial characterisation of
435 U and Pb within the sample and also provides the petrographic and compositional context
436 to assess mineral growth mechanisms and alteration textures that are critical for linking
437 dates to processes.

438

439 5.1. Non-destructive techniques

440 A range of non-destructive imaging techniques is available for sample imaging (see Figure
441 7), including cathodoluminescence (CL), back-scattered electron imaging (BSE), charge-
442 contrast imaging (CCI), and etch-track or digital autoradiography techniques. The latter, in
443 particular storage-phosphor imaging plate autoradiography and direct beta-imaging
444 autoradiography, have been documented previously and are established techniques for
445 meteoric carbonates such as speleothems (e.g. Cole et al., 2003; Woodhead et al., 2012).
446 In carbonate minerals, CL intensity is related to trace element contents but not specifically
447 U concentration. CL brightness is generally ascribed to a number of emitters, with Mn^{2+}
448 being the most dominant luminescence activator and Fe^{2+} being the dominant
449 luminescence quencher in calcite and dolomite (e.g. Machel, 1985, 2000; Savard et al.,
450 1995), although rare earth elements (REE) such as Eu^{2+} , Eu^{3+} , Dy^{3+} , Sm^{3+} and Tb^{3+} along
451 with Pb^{2+} may also activate luminescence in some cases (Richter et al., 2003). Despite not
452 being directly related to U, the very high spatial resolution of CL is useful for identifying μm -
453 scale calcite crystal growth zonation and alteration, and for characterising different mineral
454 generations formed from different fluids (e.g. Barnaby & Rimstidt, 1989; Tullborg et al.,
455 2008; Milodowski et al., 2018).

456

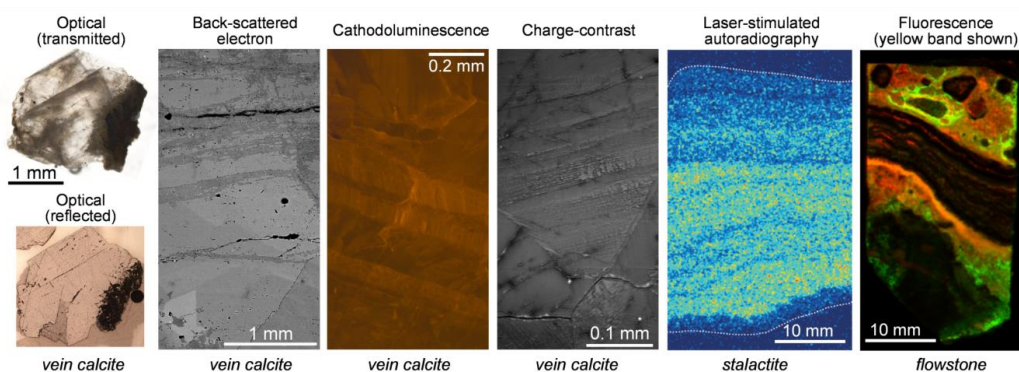
457 BSE imaging also does not correlate directly to trace concentrations of U, but to the mean
458 atomic number of the mineral. It is useful as an imaging tool for characterising zonation,
459 alteration and growth patterns, although we note that the contrast in zonation largely
460 reflects variations in major element composition, and as such it is typically less sensitive



461 than with CL. Ukar & Laubach (2016) provide a recent review of high-spatial resolution
462 SEM-based imaging of vein-filling calcite mineralisation.
463
464 CCI under the SEM directly images differences in dielectric properties, which produce
465 charge or conductivity contrasts in the near-surface of the sample that are detected by the
466 secondary electron emission, and may reflect compositional variations or strain induced by
467 deformation (Watt et al., 2000; Robertson et al., 2005). It is an underutilised method for
468 geological materials, although the exact origin of charge-contrast is poorly understood.
469 However, it can provide useful information on crystal growth, compositional zoning and
470 microstructural features, and CCI has previously been applied to garnet (Cuthbert &
471 Buckman, 2005), feldspar (Flude et al., 2012), limestone (Buckman et al., 2016) and
472 biogenic calcite (Lee et al., 2008). The technique requires very clean and carefully-prepared
473 and polished sample surfaces because it is sensitive to surface contamination and
474 mechanical defects, and imaging needs to be undertaken on uncoated samples under low-
475 vacuum conditions.
476
477 In addition to the microscopy-based methods listed above, a lower resolution but potentially
478 useful technique is provided by storage-phosphor imaging-plate (IP) autoradiography using
479 a plastic support film coated with a photostimulated phosphor (BaFBr:Eu²⁺) (Hareyama et
480 al., 2000). This technique records an image of the spatial distribution and intensity of total
481 radioactivity (from alpha, beta and gamma emitters) from a flat sample surface. In natural
482 geological materials, IP radiography records radioactivity from U, Th (and their radioactive
483 daughters), ⁸⁷Rb, and ⁴⁰K (Hareyama et al., 2000; Cole et al., 2003). Although U is not
484 specifically discriminated, it has been shown to be a useful screening tool for finding U-
485 bearing domains in carbonate materials (Cole et al., 2005). The method has been
486 particularly applied to speleothem studies where its large sample-size capabilities (up to at
487 least 40 cm) are beneficial. Spatial resolution is a few tens of micrometres, depending on
488 the pixel size of the laser scanner. However, the detection limit depends on the exposure
489 time of the IP in direct contact with the sample surface: routinely this is around 14-28 days
490 giving a detection limit of a few ppm U, which is typically higher than many carbonate
491 samples. Whilst this may be suitable for speleothems, which typically have higher uranium
492 concentrations, we do not regularly adopt the method for very low U contents in vein-filling
493 or diagenetic carbonates.
494



495 Fluorescence imaging has long been used in defining and characterising growth fabrics in
496 speleothems, although it does not specifically identify U-rich regions. This usually involves
497 irradiating a sliced sample with UV-light and observing the excited fluorescence emission at
498 a longer (visible light) wavelength, using either a standard UV microscope or digital
499 scanning with a UV laser system (e.g. Shopov et al., 1994; Baker et al., 1995; 2008;
500 Perrette et al., 2005). Fine growth detail with spatial resolutions of between 50 to 100 μm
501 are achievable. Speleothem fluorescence under UV at excitation wavelengths of 300-420
502 nm is dominated by the intrinsic fluorescence of natural high molecular weight and aromatic
503 organic (“humic” and “fulvic”) compounds, with emission between 400-480 nm (Baker et al.,
504 2008). However, we have also successfully imaged speleothems (Figure 7) and other
505 geological materials (Field et al., 2019) by direct laser-stimulated scanning fluorescence
506 imaging (LSSFI) using 635 nm (red) and 450 nm (blue) wavelength excitation with 650 nm
507 and 520 nm low-pass wavelength filters, respectively. Although, such equipment is
508 principally applied to imaging of biological materials labelled with organic fluorescent dyes
509 (fluorochromes) (e.g. fluorescein), it is able to image variations in fluorescence originating
510 from organic laminae and subtle differences between carbonate minerals (calcite,
511 aragonite), revealing microtextural details with a resolution of about 100 micrometres.
512



513
514
515
516
517
518

Figure 7. Example imagery from the range of techniques used for sample screening and characterisation.



519 5.2. Destructive techniques

520 Several approaches for destructive sample screening using LA-ICP-MS are available.
521 These can include either systematic or non-systematic (random) spot traverses across
522 carbonate samples, and can include full analyses (i.e. a 30 second ablation following a pre-
523 ablation) or a much shorter analysis time (with or without pre-ablation). We commonly adopt
524 systematic traverses across samples utilising shorter ablation times but including a pre-
525 ablation, so as to avoid common Pb from the surface. This is a quick way to determine with
526 reasonable precision and accuracy whether a sample is a single age population that
527 represents a closed isotopic system with a suitable range in μ . For some samples, this
528 provides potentially useable age information that does not require any further refinement
529 (e.g. Figure 5H-5I). Conversely, this may provide a population of data that exhibits no
530 potential, i.e. dominated by common-lead (e.g. Figure 5A-5B), open-system behaviour (e.g.
531 Figure 5D), or mixed analyses (e.g. Figure 5C). Screening in this way allows us to analyse
532 several samples or sample-aliquots in a single LA-ICP-MS session, and thus identify the
533 material most likely to provide an accurate and precise age.

534

535 Either as an alternative to spot traverses, or subsequent to spot traverses, we use LA-ICP-
536 MS mapping to determine both the location and nature of U and Pb zonation in the
537 carbonate material. Whereas spot traverses provide rapid screening of multiple
538 samples/aliquots, mapping provides fairly rapid (5 x 5 mm in < 2 hours) screening across
539 complexly zoned samples. Different approaches can be adopted, a suite of major and trace
540 elements can be analysed alone, a suite of elements for age determination (i.e. Pb to U \pm
541 Hg) can be measured, or, depending on ICP-MS instrumentation, these can be combined,
542 i.e. using a quadrupole ICP-MS (Drost et al., 2018) or a split-stream set-up utilising two
543 ICP-MS instruments (e.g. Kylander-Clark et al., 2013). As will be shown by the examples in
544 the subsequent sections, trace element maps are useful for directly comparing U and Pb
545 zonation with other trace and major elements. We have found that in primary vein-filling
546 calcite, U typically correlates with other trace elements, this varies between samples, but
547 can include V, Mn, Y, and the REEs. We can use this information to distinguish primary
548 zones of calcite from those that have been altered (see Section 5). Elements, or elemental
549 ratios such as Ba/Ca, can be used to distinguish alteration zones or secondary material
550 (e.g. a detrital component). For example, in meteoric carbonates, high Th is commonly
551 attributed to detrital matter. The production of trace element maps rapidly produces extra
552 information that can be related to any later age determination, facilitating the relating of the



553 age to a specific growth event, i.e. the petrochronological approach (i.e. Kylander-Clark et
554 al., 2013; Engi et al., 2017).

555

556 An alternative approach is to produce maps that generate U-Pb data directly (see Section
557 5.5). These have obvious utility in determining suitable domains of calcite; however, for
558 common-lead bearing minerals they can be difficult to interpret by visual inspection. Pb-Pb
559 or Pb-U isotope maps can be created with ease; however, because of the inherent inclusion
560 of common lead, more useful is a map of common lead-corrected $^{206}\text{Pb}/^{238}\text{U}$ ages or ratios.
561 Common lead-corrected age maps require: 1) precise knowledge of the initial lead
562 composition (or upper intercept in Tera-Wasserburg space); and 2) knowledge that the
563 initial Pb composition is homogeneous across the mapped region, something that is not
564 always the case (see Section 5.4). However, with the recent advent of more advanced data
565 processing software, such as the Monocle plug-in for lolite (Petrus et al., 2017), complex
566 age determination from maps is becoming more amenable (see Section 5.5). The caveat
567 with such data processing packages is that non-related domains defining a single age with
568 a good precision can potentially be selected with subjectivity, and without relation to actual
569 geological/mineralogical process. For this reason, we suggest that it is imperative that users
570 relate domains they have selected for U-Pb age determination to specific mineralogical
571 domains that can be identified independently with other means, whether these be entire
572 crystals, domains of crystals, growth bands, or specific veinlets. As suggested by Drost et
573 al. (2018), who demonstrate the method for carbonate sediments, it is also useful to
574 compare conventional spot ablation analyses with the map-generated dates to verify the
575 accuracy of the latter.

576

577 **6. Analytical Protocol**

578 The LA-ICP-MS method for carbonate follows a typical sample-standard bracketing
579 approach using a matrix-matched reference material, i.e. as for other silicate or phosphate
580 minerals (e.g. zircon, monazite, titanite, rutile, apatite, allanite), with only minor
581 modifications. Similarly, uncertainty propagation and data reporting should follow the
582 community-based guidelines for zircon of Horstwood et al. (2016). Details on the LA-ICP-
583 MS method for carbonate adopted by three major laboratories taking a similar approach are
584 provided in Roberts & Walker (2016) and Drake et al. (2017) for the British Geological
585 Survey laboratory (Nottingham, UK); Ring & Gerdes (2016) and Methner et al. (2016) for



586 Goethe-Universität (Frankfurt, Germany), and Nuriel et al., (2017, 2019) for University of
587 California Santa Barbara (Santa Barbara, USA). There are two key points of the method we
588 feel are worth highlighting that differ from 'standard' methods based on silicate minerals
589 such as zircon. Firstly, the heterogeneous nature of the Pb isotope composition of matrix-
590 matched, i.e. calcite/dolomite, minerals (due to variable common Pb incorporation), means
591 that normalisation of the Pb-Pb isotope ratios is currently achieved using a synthetic glass
592 rather than a carbonate, typically NIST612 or NIST614. At present, there is no evidence to
593 suggest that the Pb/Pb mass bias is variable across different matrices. Secondly,
594 calculation of the reproducibility of the primary and secondary matrix-matched reference
595 materials, which is required for uncertainty propagation (Horstwood et al., 2016) and
596 determination of the true method accuracy and precision, is hindered by the fact that the
597 carbonate reference materials currently employed have U/Pb heterogeneity that is equal to
598 or much larger than the analytical uncertainties (Roberts et al., 2017). This means there will
599 typically be a significant excess variance of the reference material U/Pb isotope
600 measurements in any one session (including after correction for common lead), which does
601 not describe the reproducibility of the analytical system but instead reflects the natural
602 variation in the reference material. If propagated onto the sample data-point uncertainties
603 as a within-session excess variance as recommended for zircon in Horstwood et al (2016),
604 these data point uncertainties will be overestimated masking any smaller scale, real
605 geological scatter in the sample isochron and result in meaningless ages with erroneously
606 high precision. For this reason, it is suggested that calculation of the session-based
607 reproducibility is best estimated using a more homogenous material such as NIST glass or
608 zircon. However, it should be noted that through this practice results can only be compared
609 in a relative sense within session, or between sessions if validation materials are compiled
610 and used. To compare data in an absolute sense, i.e. to assign an age and total uncertainty
611 to a material for comparison between laboratories and/or with other methods, the
612 uncertainty from the primary reference material must be included to reflect the accuracy
613 with which the matrix-matched normalisation is known. In this way, the uncertainty of the
614 primary reference material constitutes a limiting uncertainty on any sample age. Improved
615 reference materials with less scatter around the U/Pb isochron are therefore a pre-requisite
616 for improving this method.
617



618 **7. Generating U-Pb data and interpreting ages**

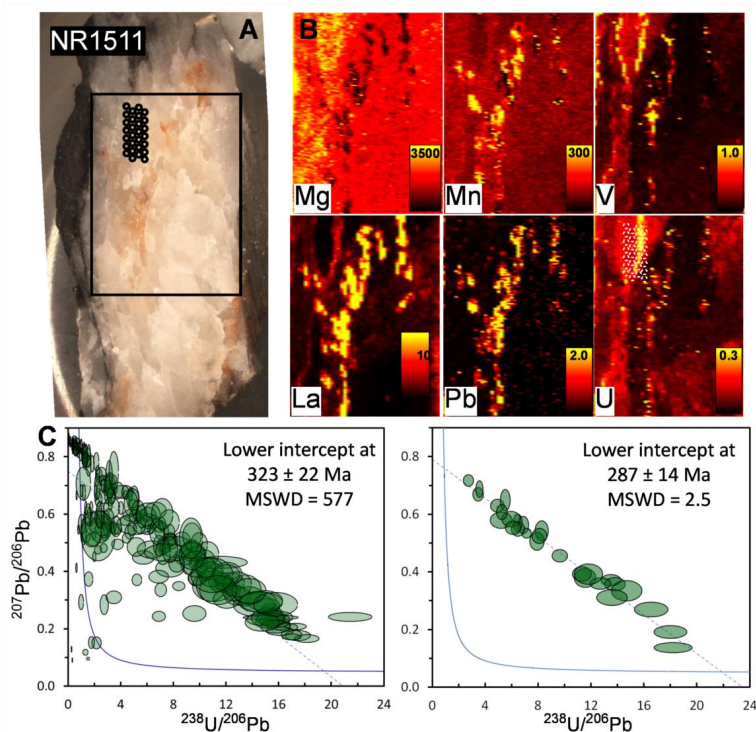
619 Generating ages and relating these to geological processes requires the marriage of
620 spatially-resolved variations in composition (elemental and isotopic) and U-Pb isotopic
621 concentrations. In this section, we present several case studies to highlight our approach to
622 dating vein-filling calcite, the potential applications to dating faulting and fluid-flow, and the
623 type of material commonly encountered. First we present the standard approach, which
624 used independent imagery and analysis to target, refine, and interpret the U-Pb analyses
625 that are based on static spot ablations. This is the same approach as using CL imagery to
626 help interpret zircon dates, and that can be further refined with information such as
627 companion trace element data. A second approach (age mapping) is to use mapping tools
628 not just to image the sample and its composition, but to extract age data from the map itself
629 (Petrus et al., 2017; Drost et al., 2018).

630

631 7.1. Image-guided dating

632 *Example A - Variscan-related veins in the Northumberland Basin*

633 Figure 8 shows U-Pb calcite data from Howick Bay in the Northumberland Basin, NE
634 England. The mudstone succession in the bay is faulted and weakly folded, which is
635 postulated to be a result of transpressional stress during the Variscan orogeny (De Paola et
636 al., 2005). Syn-kinematic calcite located within fractures has the potential to date this far-
637 field intraplate deformation (c.f. Parrish et al., 2018). Screening data from one sample,
638 comprising randomly located spot traverses across a crystal, are presented in Figure 8C.
639 The data yield a regression with a large array of common to radiogenic Pb compositions,
640 but with significant scatter (MSWD = 577), indicating some alteration and open-system
641 behaviour and/or mixed age domains. The crystal was subsequently mapped for its trace
642 element distribution, revealing a zone of low Ca and Mg, and high Mn, REEs and Pb. This
643 zone can be seen optically, and is interpreted as a zone of alteration. Further U-Pb spot
644 analyses were placed in a domain away from this feature that exhibits high U, with the data
645 yielding a more precise regression with an age of 287 ± 14 Ma (MSWD = 2.5). This
646 example highlights the use of trace element mapping to locate regions of highest U, to
647 assist and refine U-Pb analyses, and shows the potential for dating calcite veins into the
648 Palaeozoic.
649



650

651 *Figure 8. A) Photomicrograph of sample NR1511 showing position of mapped area and*
652 *ablation spots (in black); B) Trace element maps generated with LA-ICP-MS using line*
653 *rasters, the scales are in ppm and white spots show the ablation locations; C) Tera-*
654 *Wasserburg concordia of U-Pb data from this sample based on screening spot traverses;*
655 *D) Tera-Wasserburg concordia of U-Pb spot data placed using constraints from map data,*
656 *i.e. over the unaltered high U region.*

657

658

659 *Example B - Faroe Island vein mineralisation*

660 The aim of most studies is to date primary calcite formation rather than subsequent
661 secondary alteration, particularly when dating syn-kinematic calcite for constraining the
662 timing of fault slip (e.g. Roberts & Walker, 2016; Ring & Gerdes, 2016; Goodfellow et al.,
663 2017; Hansman et al., 2017; Nuriel et al., 2017, 2019; Parrish et al., 2018; Holdsworth et
664 al., 2019; Smeraglia et al., 2018). Trace element mapping is a useful tool to assist with
665 identification of growth zoning, particularly on the scale of mm- to cm-sized chips. Using
666 standard LA-ICP-MS protocols for trace element determination, with standard-sample



667 bracketing routines, a 5 x 5 mm region can be mapped in less than two hours. As discussed
668 previously, depending on the analytical set-up, this trace element mapping can be
669 conducted alongside U-Pb isotope mapping.

670

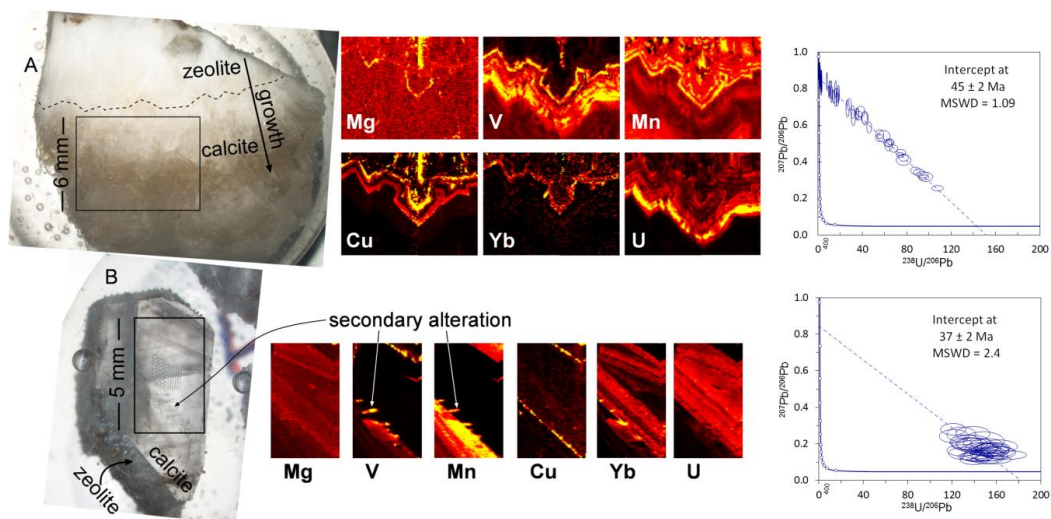
671 Figure 9 shows selected results from dating of syn-kinematic crack-seal-slip calcite
672 mineralisation from basalt-hosted faults of the Faroe Islands (Roberts & Walker, 2016).
673 Sample A is from a vein exhibiting a zeolite-calcite-zeolite mineral paragenesis. The calcite
674 exhibits distinct syntaxial growth zoning towards the centre of the vein. Trace element
675 mapping reveals large variation in trace element contents in the direction of growth,
676 interpretable as changing metal/Ca ratios in the mineralising fluid (e.g. Drake et al., 2014).
677 The trace element zonation clearly follows the optically visible growth zonation, indicating
678 its primary nature. Uranium increases steadily to the maximum concentrations observed,
679 then abruptly drops to very low abundances. The U-Pb data define a well-behaved isochron
680 (low scatter with large spread in U/Pb ratios), determined from spots placed on and near
681 the high U region, and yields a lower intercept U-Pb age of 45 ± 2 Ma (MWD = 1.09).

682

683 Sample B is from a large dilational jog (up to 1 m wide) that is filled with zeolite-calcite-
684 zeolite mineralisation, including calcite crystals up to 10 cm long. The mapped grain is
685 composed of calcite with a later rim of zeolite. Trace element mapping reveals a strong
686 correlation between most elements, again, representing the primary growth zonation. High
687 Mn and V 'fingers' intersect the growth zonation, and are visible optically. We interpret
688 these as pathways of secondary alteration. Given that the vein exhibits vuggy textures, it is
689 possible that fluids have precipitated or altered the original calcite much later than the
690 original fault slip. U-Pb analyses of the primary calcite in this sample reveal fairly radiogenic
691 Pb compositions, although with large datapoint uncertainties owing to the low U
692 concentrations, with a lower intercept U-Pb age of 37 ± 2 Ma (MSWD = 2.4; anchored
693 upper intercept based on other samples on this study at 0.89 ± 0.02). Trace element
694 mapping allows us to visualise and fingerprint these alteration zones, and avoid or remove
695 them from analyses used for dating. A benefit to this approach is that the maps can then be
696 used to estimate the trace metal contents of the mineralising fluids, which in turn provides
697 information about rock-water interaction and the redox conditions for example. These maps
698 also demonstrate that no measurable diffusion of trace elements across the calcite crystals
699 has occurred over a significant time span, as the distribution is interpreted as a primary
700 feature.



701



702

703

704 *Figure 9. A) Sample microphotographs of epoxy-resin mounted zeolite-calcite vein*
705 *samples, TJN-0-1 and TJN-6-1, mapped regions shown in black; B) Trace element maps*
706 *generated with LA-ICP-MS using line rasters; C) Tera-Wasserburg concordia of U-Pb data*
707 *from each sample (from Roberts and Walker, 2016).*

708

709

710 *Example C - Sellafield fracture mineralisation*

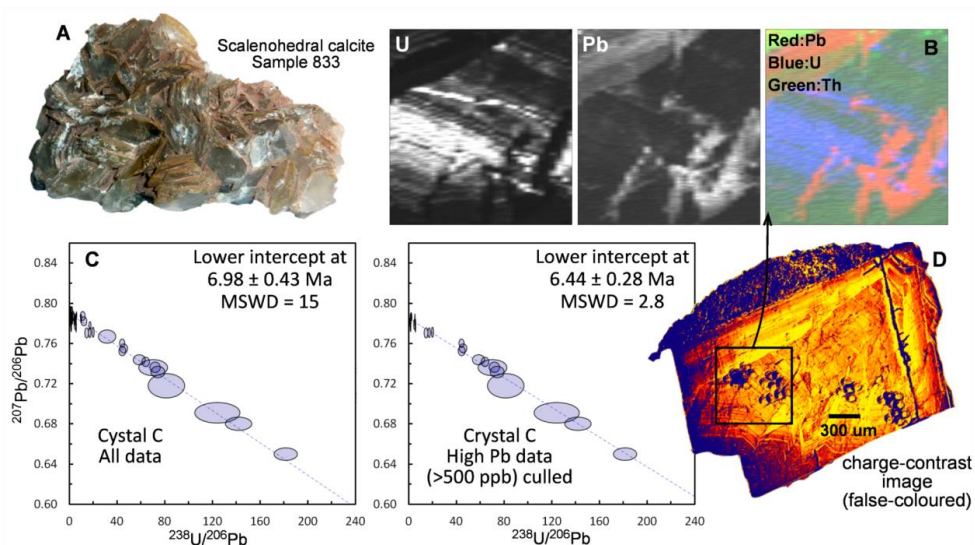
711 Figure 10 shows results for fracture mineralisation from Sellafield, NW England. This
712 location was previously investigated (1990-1997) as a potential nuclear waste repository
713 site, and has thus been extensively studied in terms of its structure, stratigraphy,
714 geochemistry and palaeo- to present-day hydrogeology (Michie & Bowden, 1994; Akhurst
715 et al., 1997; Baker et al., 1997; Heathcote and Michie, 2004; Bath et al., 2006; Milodowski
716 et al., 1998, 2018). Deep (up to 2 km) site-investigation boreholes revealed a complex
717 sequence of fracture mineralisation within Ordovician greenschist-facies metamorphic
718 basement rocks overlain by Carboniferous Limestone and Permo-Triassic sedimentary
719 strata (Milodowski et al., 1998). Presented here are data from one mineralised zone that
720 show the potential for U-Pb dating of such material.

721

722 Sample 833 is an example of euhedral calcite crystals lining open fractures and
723 representing the latest mineralisation, and which are very closely-associated with the



724 present-day fracture-controlled groundwater system (generation ME9 of Milodowski et al.,
725 1998; 2018). The sample has U and Pb concentrations of 0.3—30 ppm and 0.1—3.6 ppm,
726 respectively. U-Pb LA-ICP-MS spot analyses were placed in a single crystal which was
727 optically continuous; the data yielded an age of 6.98 ± 0.43 Ma (MSWD = 15). The dated
728 crystal was subsequently mapped for its U, Th and Pb elemental distribution using LA-ICP-
729 MS. The map shows zoning of U, Th and Pb that is interpreted as growth zoning during
730 primary calcite growth. Pb is distributed similarly, but with high concentrations along narrow
731 veins that are discordant to the primary growth zoning; these are interpreted as alteration
732 pathways where Pb-bearing fluids have invaded the crystals. Crystals were also imaged
733 using charge-contrast imaging (CCI), which highlights structural imperfections in the calcite
734 crystals. The same veinlets that have elevated Pb concentrations are imaged as cracks and
735 disturbances to the growth zoning. Since the spots that lie on the alteration pathways have
736 high Pb counts, the age data were culled based on Pb concentration (>500 ppb Pb
737 removed). This approach reduced the scatter in the regression, presumably removing
738 components with slightly different common lead compositions, giving a more precise age of
739 6.44 ± 0.26 Ma (MSWD = 2.8). These data from Sellafeld demonstrate the potential utility
740 of imaging techniques such as CCI and trace element mapping to discriminate primary
741 growth domains from those that are altered at the micro-scale (<100 μm), and refinement of
742 scattered analyses into those that are interpretable as a single population.
743



744



745 *Figure 10. A) Photograph of sample 833; B) Trace element maps using LA-ICP-MS based*
746 *on line rasters; C) Tera-Wasserburg concordia of U-Pb data before and after refining the*
747 *data; D) False-colour charge-contrast image of the dated crystal, showing the mapped*
748 *region in black.*

749

750 7.2. Age mapping of vein-fill carbonates

751 We have demonstrated that elemental mapping data are useful for refining and interpreting
752 U-Pb isotopic data. For example, in Example B above, we manually located the spots in a
753 high U zone, and in Example C, we manually removed the data with high Pb
754 concentrations. An alternative approach to using the maps to ‘manually’ locate spots or
755 refine spot data, is to generate a combined elemental and U-Pb isotopic 2D dataset (i.e.
756 map); the benefit of this method is that software tools can be used to both discriminate
757 specific isotopic data based upon chosen criteria, and also to show regions within these
758 pooled datasets that have similar compositional characteristics. *Iolite* (Paton et al., 2011) is
759 one of the most commonly used data reduction tools for both U-Pb isotopic data (Paton et
760 al., 2010), and for generation of elemental 2D maps. *Monocle* is a software plug-in for *Iolite*
761 that allows the user to generate maps of isotopic and elemental data (Petrus et al., 2017),
762 and to define and extract regions of pooled compositional data, including those used for
763 age calculations. Drost et al. (2018) demonstrated the efficacy of the software for dating
764 carbonate sediments, whereby features such as bioclasts and detrital components are
765 removed. For a detailed explanation of the protocol, see Drost et al. (2018). In brief, each
766 pixel of the elemental and isotope ratio maps corresponds to one duty cycle of the ICP-MS.
767 First, pixels are removed, using user-defined selection criteria that are believed to be
768 related to alteration, secondary material, or a younger or older carbonate generation. This is
769 usually conducted after an initial inspection of the mapping data combined with prior
770 imaging and petrography; however, the screening can also employ an iterative approach
771 after generation of initial U-Pb isochrons. After this screening/filtering, the remaining data
772 are pooled into a number of pseudo-analyses (each corresponding to the same number of
773 pixels) based on a suitable isotope ratio, such as $^{238}\text{U}/^{208}\text{Pb}$ or $^{235}\text{U}/^{207}\text{Pb}$. The pooling is
774 achieved using an empirical cumulative distribution function (ECDF) to maximise the spread
775 in U/Pb ratios, and an appropriate number of pixels to produce a reasonable population of
776 data, for example twenty to forty data-points. Here, we present examples of this approach
777 applied to vein-filling calcite.

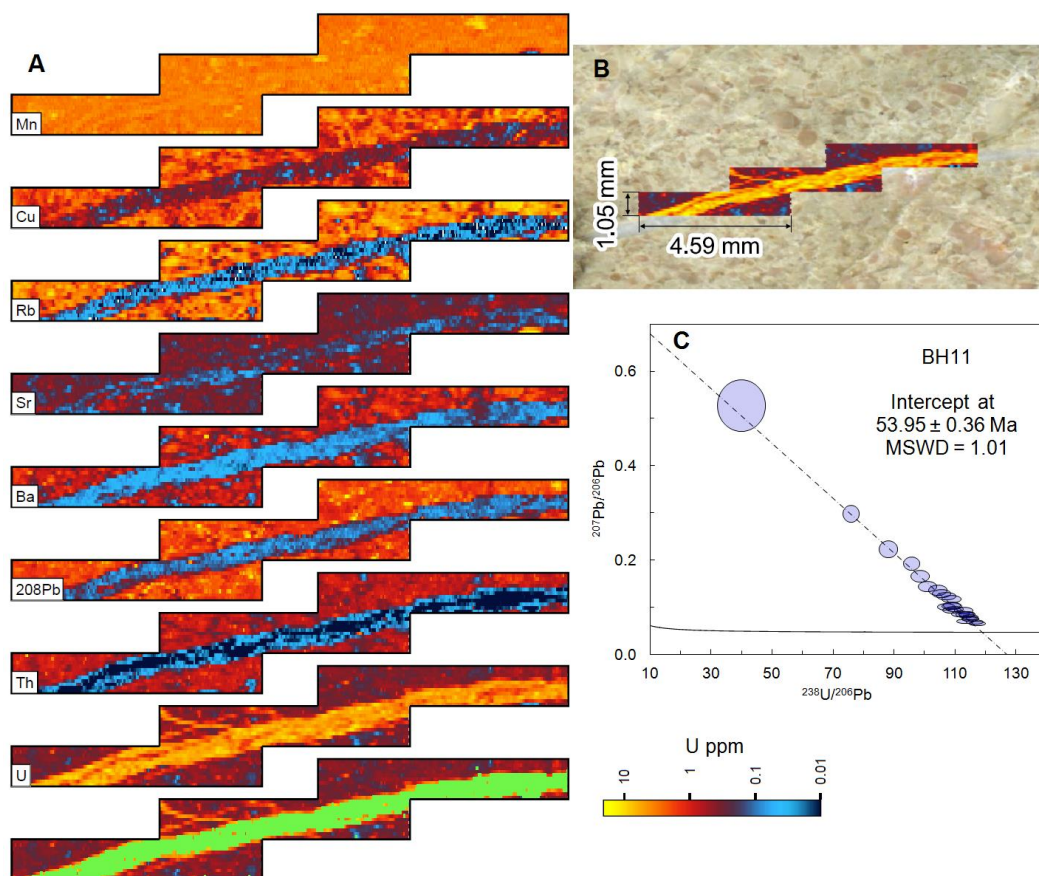


778

779 *Example D – BH11*

780 This example is of a fine-scale vein cross-cutting a sedimentary host rock; the objective is
781 to use Monocle-based criteria to discriminate the vein from the host rock and determine a
782 robust age. Only two criteria of filtering were needed to distinguish the vein from the host:
783 Mg of less than 5000 ppm, and Th of less than 0.1 ppm. The remaining data were pooled
784 using $^{238}\text{U}/^{208}\text{Pb}$ ratios into 26 analyses, and yielded a robust lower intercept $^{238}\text{U}/^{206}\text{Pb}$
785 date of 53.95 ± 0.36 Ma, with an MSWD of 1.0 (Figure. 11). This sample was previously
786 dated using conventional spot analyses located within the vein at 53.51 ± 0.39 Ma (MSWD
787 = 2.0; Beaudoin et al., 2018). These dates, quoted without propagation of systematic
788 uncertainties, show good agreement between two different labs using different
789 instrumentation and data reduction methods.

790



791



792 *Figure 11. Image-based dating (Monocle plug-in for Iolite) of sample BH11. A) Trace*
793 *element maps of the analysed region, the final map shows the region of interest selected*
794 *for the U-Pb date highlighted in green; B) Photomicrograph of the sample surface showing*
795 *the mapped region as a U map; C) Tera-Wasserburg concordia of U-Pb data after pooling*
796 *and filtering using the Monocle plug-in (see text for description).*

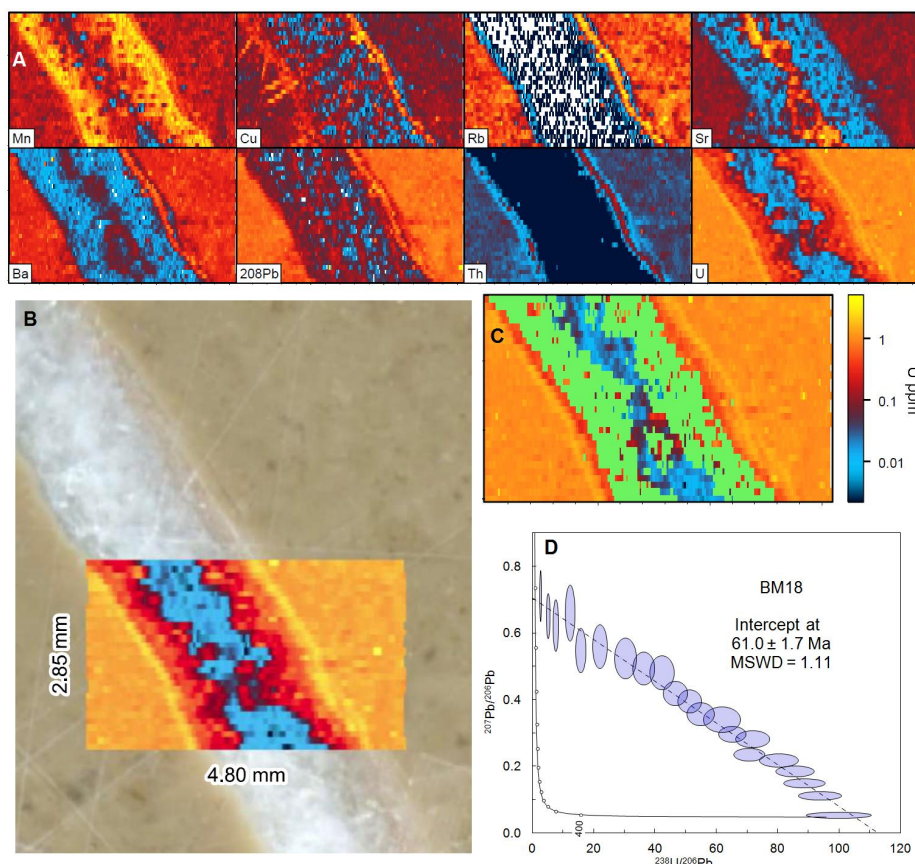
797

798

799 *Example E – BM18*

800 BM18 is another example of a vein cross-cutting a sedimentary host-rock. This time, there
801 is clear zonation of the vein (Figure. 12). Since it is a syntaxial vein (crystals growing from
802 the wall rock to the centre), this zonation probably represents changing fluid chemistry as
803 the calcite crystals were precipitating. However, it could represent multiple generations of
804 calcite precipitation. Criteria were selected for filtering of the data to highlight the outer
805 regions of the vein; Rb < 0.05 ppm, Th < 0.01 ppm, and Sr < 400 ppm. The U-Pb data were
806 then filtered to remove data with low U and Pb signals, since no initial rejection of data
807 based on detection limit was conducted using this data reduction method; criteria for
808 acceptance were $^{238}\text{U} > 500$ cps, and $^{207}\text{Pb}/^{206}\text{Pb} < 1.5$. The remaining data produce a
809 robust isochron with a lower intercept date of 61.0 ± 1.7 Ma (MSWD = 1.11; 21 pooled
810 analyses). This date overlaps that previously obtained using spot analyses that were
811 derived from the entire width of the vein (59.5 ± 1.7 Ma; Beaudoin et al., 2018).

812



813
814 *Figure 12. Image-based dating (Monocle plug-in for Iolite) of sample BM18. A) Trace*
815 *element maps of the analysed region; B) Photomicrograph of sample surface showing*
816 *mapped region as U map; C) U map showing the region of interest selected for the U-Pb*
817 *date in green; D) Tera-Wasserburg concordia of U-Pb data after pooling and filtering using*
818 *the Monocle plug-in (see text for description).*

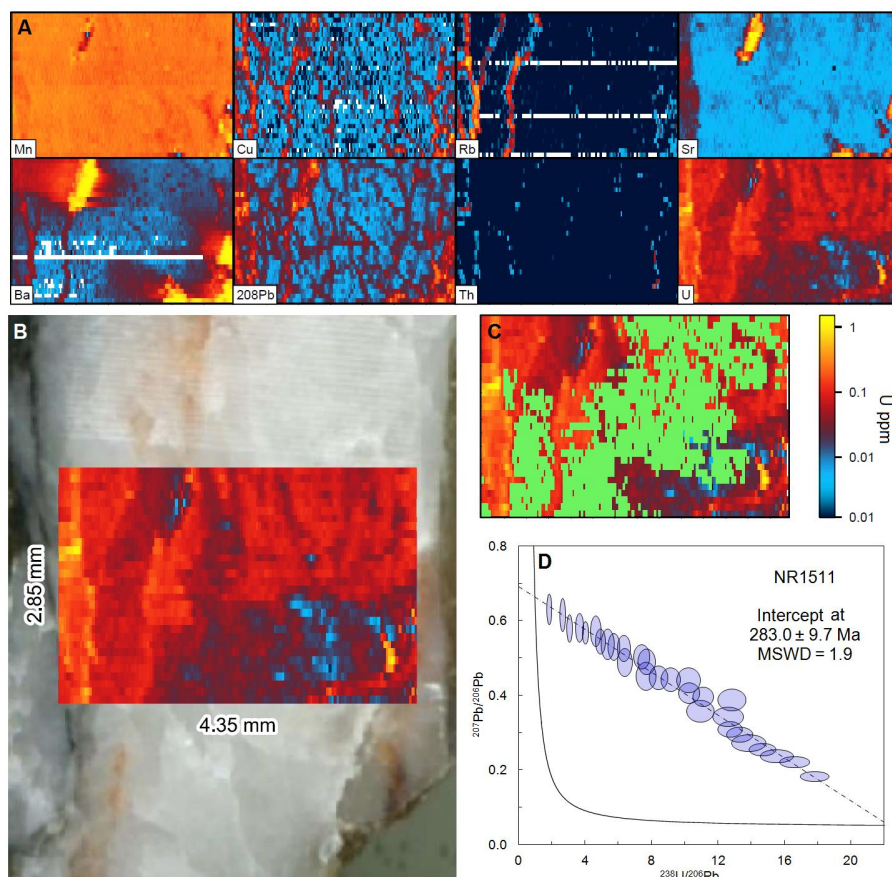
819

820 *Example F – NR1511*

821 The third example of image-based dating is from a complex vein already described in
822 section 5.1 above (Example A). This vein features visible textures and chemistry associated
823 with alteration (Figure. 13). The mapped region is entirely within the vein (no host rock).
824 High concentrations in several elements (e.g. Cu, Ba, Rb, Sr, Ba and Pb) reflect veinlets
825 that can be seen optically as a yellow altered region. The remaining portion of the vein
826 varies in U content, which likely represents chemical zonation across the coarse sparry
827 calcite growth. A fairly robust isochron (MSWD = 1.9) was obtained after filtering of the data



828 for the clearly altered regions, cleaning up the U-Pb data to remove low U and Pb signals,
829 and pooling the data based on $^{207}\text{Pb}/^{235}\text{U}$. The criteria for acceptance were: Cu < 0.2 ppm,
830 Ba < 10 ppm, Rb < 0.01 ppm, and ^{238}U < 10000 cps (for removal of alteration), and ^{238}U >
831 500 cps, $^{207}\text{Pb}/^{206}\text{Pb}$ > 0.15 < 1.5, and $^{206}\text{Pb}/^{208}\text{Pb}$ > 0.1 < 10 (for 'cleaning up' the U-Pb
832 data). These data yielded a date of 283 ± 9.7 Ma, which overlaps that obtained from spot
833 analyses and manual location of the spot data based on prior LA-ICP-MS mapping ($287 \pm$
834 14 Ma; see Figure 8D), but with an improvement in the precision (4.9 to 3.4 %).
835



836
837 *Figure 13. Image-based dating (Monocle plug-in for lolite) of sample NR1511. A) Trace*
838 *element maps of the analysed region; B) Photomicrograph of sample surface showing*
839 *mapped region as U map; C) U map showing the region of interest selected for the U-Pb*
840 *date in green; D) Tera-Wasserburg concordia of U-Pb data after pooling and filtering using*
841 *the Monocle plug-in (see text for description).*
842



843 **8. Isotopic composition of common lead**

844 Carbonates nearly always take up some amount of lead during their formation, referred to
845 as 'common' or initial lead. Contamination during handling (i.e. during cutting and polishing)
846 or from recent exposure to the environment will have a modern isotopic composition of
847 common lead, i.e. approximating the Stacey & Kramers (1975) model for terrestrial lead
848 composition at present-day, roughly $^{207}\text{Pb}/^{206}\text{Pb} = 0.84$. Distinguishing between such
849 contamination and the common lead incorporated during formation can be difficult. Well
850 behaved U-Pb isotopic systematics in a carbonate sample should yield a single mixing line
851 between the common and radiogenic end-members, and ideally will have enough spread in
852 U/Pb ratios to yield a precise regression with low uncertainties at both the lower (radiogenic
853 lead) and upper (common lead) intercepts. However, many samples will exhibit a lack of
854 spread in U/Pb ratios, or will be dominated by radiogenic compositions (e.g. Figure 5F).
855 Although a best-fit line may be calculated for such data, the slope, and thus age, may be
856 inaccurate. Thus, it is useful for such samples to have an estimation of the common lead
857 composition through other means, such as from nearby cogenetic samples formed at the
858 same age, or from different minerals also believed to have been formed at the same age.
859

860 For some mineral chronometers, such as the phosphate mineral monazite, it is common to
861 use an estimate of the common lead composition based on the Stacey and Kramers (1975)
862 model (e.g. Palin et al., 2013; Regis et al., 2016). In our experience, this is an acceptable
863 approach because from a number of different studies, we find that the common lead
864 composition determined from other minerals (i.e. feldspar, biotite, apatite) overlaps the
865 Stacey and Kramers (1975) composition (e.g. Stübner et al., 2014; Warren et al., 2014). For
866 carbonate however, we find this is not always such a suitable approach. Our experience
867 from hydrothermal carbonate in particular, is that common lead compositions are often
868 more radiogenic (lower $^{207}\text{Pb}/^{206}\text{Pb}$ ratios) than the terrestrial lead model (Stacey and
869 Kramers, 1975) for age of carbonate crystallisation. This can occur if the carbonate has
870 incorporated lead during its formation that is derived from ancient sources. Figure 14 shows
871 a compilation of common lead intercepts from a number of studies of fracture-filling calcite
872 (compilation of BGS laboratory data). The data represent different host lithologies, different
873 ages (dominated by Cretaceous to Miocene), and different geological regions. It is clear
874 that for many samples in this compilation, anchoring at a value close to the terrestrial lead
875 model composition for Phanerozoic ages, i.e. $^{207}\text{Pb}/^{206}\text{Pb} \sim 0.84$, will lead to calculated
876 ages older than the true age due to steepening of the regression. The importance of the



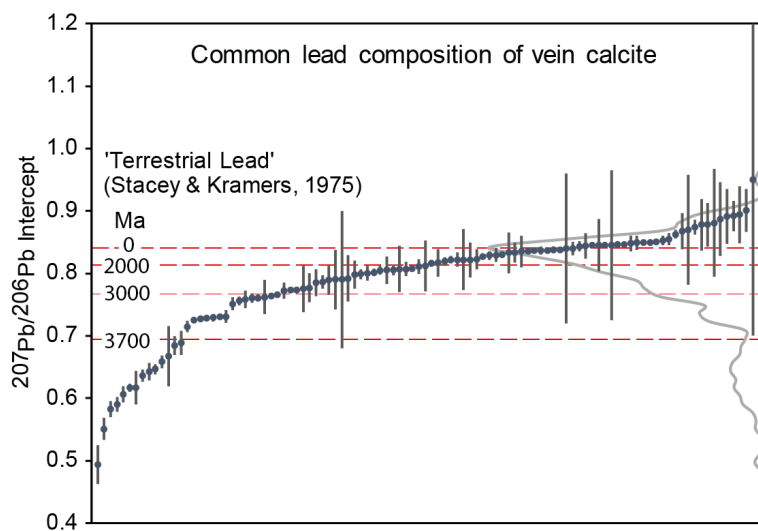
877 common lead composition in providing constraints on a calculated age will depend on the
878 amount of measured radiogenic lead in a given sample; samples dominated by common
879 lead and lacking in radiogenic lead will need a well defined array to produce a confident
880 lower intercept. We find that within individual vein samples, the apparent composition of the
881 common lead end-member can vary, limiting the precision of the regression and derived
882 age. For speleothems, Woodhead et al. (2012) demonstrate that most samples analysed in
883 their lab yield common lead compositions overlapping Stacy and Kramers (1975), and thus
884 their ages are largely insensitive to the common lead compositions. This likely reflects the
885 fact that they are precipitated from meteoric water that reflects the regional upper crustal Pb
886 composition. Although, they add the caveat that samples with $^{238}\text{U}/^{206}\text{Pb}$ below 1300
887 (equivalent to $\mu \approx 20,000$), have large inaccuracies.

888

889 The highly radiogenic initial lead values ($^{207}\text{Pb}/^{206}\text{Pb} < \sim 0.75$) recorded in our compilation
890 are mostly from two settings, young fractures in Proterozoic crystalline crust of Sweden ($n =$
891 10 of 104), and young fractures in the Bighorn Basin that overlies Archaean basement ($n =$
892 24 of 104). In both cases, the whole-rock Pb, although ancient, is not radiogenic enough to
893 produce the measured values. Instead, leaching of lead from uraniferous minerals is
894 required, e.g. titanite, allanite, monazite and zircon as a causative mechanism.

895

896



897

898 Figure 14. Compilation of upper intercept $^{207}\text{Pb}/^{206}\text{Pb}$ compositions from vein-filling calcite
899 from samples dated in the British Geological Survey laboratory ($n=104$). The grey curve is a



900 *Kernel Density Estimate showing the distribution of mean compositions. The red bars show*
901 *the two-stage Stacey and Kramers (1975) compositions of terrestrial lead at 0, 2000, 2000*
902 *and 3700 Ma. Samples with very large uncertainties in the $^{207}\text{Pb}/^{206}\text{Pb}$ composition are*
903 *those with very low Pb count-rates.*

904

905

906 *Example G - Moab fault*

907 Figure 15 shows results from a sample taken from the Moab fault in southeast Utah, USA.
908 The sample presented here (CHJ15-KH08) is collected from the Courthouse Junction fault
909 segment intersection. This locality has a complex, multi-phase deformation history
910 (Davatzes et al., 2005; Johansen et al., 2005) associated with multiple episodes of
911 mineralization and a range of diagenetic fluids (Chan et al., 2000; Eichhubl et al., 2009;
912 Bergman et al., 2013; Hodson et al., 2016).

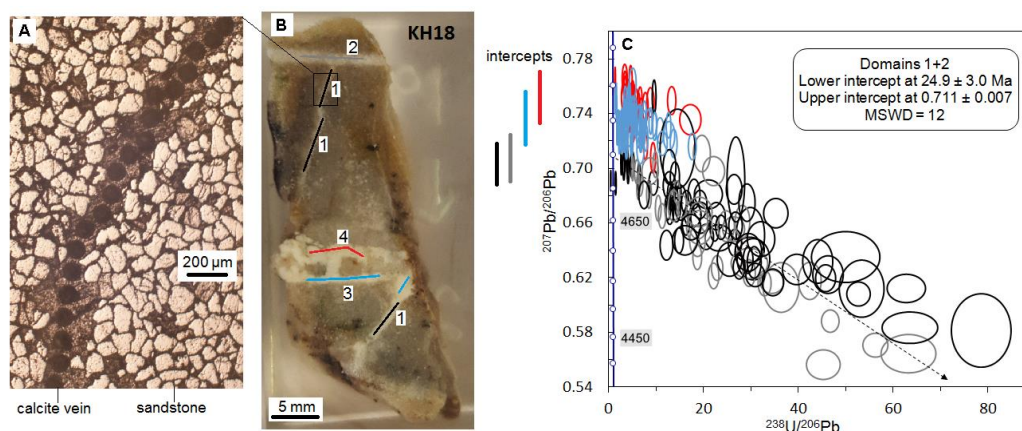
913

914 U-Pb data were obtained from different sections of the vein material formed along different
915 orientations (See Figure 15). The data exhibit a high level of common/initial lead, with
916 limited spread in radiogenic lead contents, but still forming a scattered regression to a lower
917 intercept value. Using different colours to discriminate different sections of vein, it is clear
918 that they have subtly different initial lead compositions, as indicated by the upper intercept
919 ($^{207}\text{Pb}/^{206}\text{Pb}$ value) of the data arrays. These lead compositions are different from that
920 predicted by the Stacey & Kramers (1975) terrestrial composition, which we find is a
921 common feature of many vein-filling carbonates. This is likely due to the hydrothermal fluids
922 that are precipitating the carbonate comprising unsupported radiogenic lead components
923 derived from leaching of older uraniumiferous minerals or rocks.

924

925 The existence of variable Pb compositions on small length-scales (<1 mm) means that
926 careful attention is required to interpret complex data. However, the spatial resolution of LA-
927 ICP-MS means that these details can potentially be teased out. This case study also shows
928 the potential of the method for measuring veinlets that are only ~150 μm wide (see Figure
929 15), a task that would be difficult for ID analyses.

930



931
932 *Figure 15. U-Pb data from a series of calcite veins (sample KH18) along the Moab Fault at*
933 *Courthouse Junction, Utah. A) Reflected light image of a region of veining showing the 100*
934 *μm spots; B) Photomicrograph of the dated sample, with different dated domains of veining*
935 *shown by blue, red, black and grey lines; C) Tera-Wasserburg plot with U-Pb spot data*
936 *colour-coded to match the different domains. The bars on the left show the variable*
937 *$^{207}\text{Pb}/^{206}\text{Pb}$ upper intercept values for each domain.*

938
939

940 In summary, vein-filling, diagenetic and hydrothermal carbonates often do not exhibit Stacy
941 & Kramers (1975) model Pb compositions for their assumed age, but typically yield more
942 radiogenic compositions. This means that regressions anchored with assumed common
943 lead compositions are susceptible to inaccuracy. Mixed common lead compositions in
944 samples hampers derivation of single age regressions, implying multiple fluid sources.
945 Mixed ages and atypical lead compositions can also make age mapping problematic.

946

947 **9. Dating young material – dealing with disequilibria**

948 As described in Section 3, the younger the age of the sample analysed, the lower the
949 potential for precise and accurate age determination due to the lack of radiogenic ingrowth
950 of lead. However, young carbonates are a high priority in many applications, because they
951 can date events more relevant to the Earth system at present, and because U-Pb can
952 extend the age range of sample suites or study areas where U-Th age dating is also
953 feasible. For example, records of environmental change in deep time require the dating of
954 speleothems that are older than 500 ka (see Woodhead et al., 2012, 2019), and dating of



955 veins that record seismic cycles extending beyond 500 ka (see Uysal et al., 2011; Williams
956 et al., 2017) can provide constraints on earthquakes and other hazards associated with
957 subsurface fractures. These particular applications are likely to require high levels of
958 precision, i.e. for the Quaternary, of much less than ± 100 ka, and potentially even less than
959 ± 10 ka or < 1000 years for the Holocene. Achieving such precision requires very high U to
960 achieve abundant radiogenic lead and higher μ values (see Figure 4).

961
962 A major issue for accurate dating of young samples (i.e. <10 Ma) is the potential effect of
963 initial daughter isotope disequilibrium within the uranium decay chains. The simplest form of
964 the U-Pb and Pb-Pb age equations, often used for older samples, assume that all long-lived
965 daughter isotopes in the U decay chain are initially present in secular equilibrium. Both the
966 U decay series contain long-lived daughter isotopes, including ^{234}U ($t_{1/2} = 245$ ka), ^{230}Th ($t_{1/2} =$
967 76 ka), and ^{226}Ra ($t_{1/2} = 1.6$ ka) in the ^{238}U decay chain, and ^{231}Pa ($t_{1/2} = 34$ ka) in the ^{235}U
968 decay chain. Of these, ^{234}U has the longest half life and therefore the largest potential
969 effect on U-Pb dates. The excess initial ^{234}U often observed in natural waters will lead to
970 generation of unsupported ^{206}Pb . If uncorrected, excess initial ^{234}U produces overestimated
971 $^{238}\text{U}/^{206}\text{Pb}$ and lower intercept dates. An excess of the other intermediate daughter
972 products, like ^{230}Th , relative to secular equilibrium will bias the age with a smaller
973 magnitude but in the same direction, whereas a deficit will result in dates that are too
974 young.

975
976 Carbonates are commonly precipitated from fluids containing $^{234}\text{U}/^{238}\text{U}$ out of secular
977 equilibrium. Thus, this initial disequilibrium must be considered in any age determination.
978 Age corrections for initial U daughter deficits are at maximum ~ 1.44 times the half life of the
979 daughter isotope for zero initial abundance. But for initial excesses, the age difference can
980 be many times larger (see Figure 17). For most older samples dated by U-Pb, the effect of
981 disequilibrium is deemed to be insignificant compared to larger measurement uncertainties.
982 For this reason, initial disequilibrium has thus far not been mentioned in any publication
983 concerning LA-ICP-MS U-Pb dating except for those dealing with young speleothems (e.g.
984 Hopley et al., 2019). However, here we demonstrate that initial disequilibrium may be a very
985 significant cause of uncertainty for carbonates precipitated from groundwater and other
986 crustal fluids, and not just for very young (<1 Ma) samples.

987



988 In young samples, particularly those within the range of U-Th geochronology (<600 ka), the
989 initial $^{234}\text{U}/^{238}\text{U}$ ratio ($^{234}\text{U}/^{238}\text{U}_0$) can be estimated based on the combination of the present-
990 day measured $^{234}\text{U}/^{238}\text{U}$ ($^{234}\text{U}/^{238}\text{U}_{\text{now}}$), and either the measured $^{230}\text{Th}/^{238}\text{U}$ or the estimated
991 date of formation. The robustness of this estimate is highly dependent on the precision and
992 accuracy at which the isotope ratio(s) can be measured (the atom ratio is very small,
993 making high precision measurement >1‰ difficult). In addition, if the offset between
994 $^{234}\text{U}/^{238}\text{U}_{\text{now}}$ and secular equilibrium is small, then the measurement may overlap secular
995 equilibrium within uncertainty. For this reason, the highest precision possible is a necessary
996 target for any disequilibrium correction measurement.

997

998 For older samples (i.e. those older than about four times the half-life of ^{234}U), and/or those
999 with only a small degree of initial disequilibrium, $^{234}\text{U}/^{238}\text{U}_{\text{now}}$ is likely to have reached
1000 secular equilibrium. This means that $^{234}\text{U}/^{238}\text{U}_0$ cannot be estimated from the measured
1001 data alone. One approach to alleviate this problem is to take known initial ratios from
1002 younger samples (<600 ka) formed in approximately the same geologic setting, and apply
1003 these corrections to the older samples from the same setting (e.g. Woodhead et al., 2006,
1004 2019). This approach is only applicable if the geological environment is well known and the
1005 hydrological system believed to be relatively stable.

1006

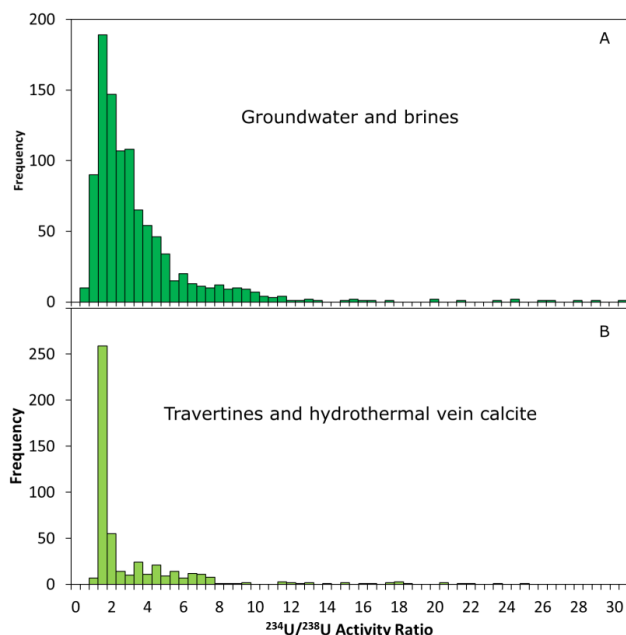
1007 There are various causes of ^{234}U excess in fluid-mineral systems, which have been studied
1008 at length (e.g. Osmond & Cowart, 1992, 2000; Porcelli & Swarzenski, 2003; Suksi et al.,
1009 2006). In summary, ^{234}U is generated from α decay of ^{238}U , and may preferentially be
1010 increased in the fluid state during mineral-fluid interaction due to oxidation state and
1011 valence differences between the U species (e.g. Suksi et al., 2006). Uranium activity ratios
1012 record information on the redox state of fluids, the source of uranium in the fluids, and
1013 potentially the timing of uranium residence in the fluid; therefore, they have long been a
1014 focus of groundwater studies (e.g. Osmond et al., 1968; Osmond & Cowart, 2000; Porcelli
1015 & Swarzenski, 2003). Of general interest here, is whether carbonates precipitated from
1016 different geological settings are likely to have significant ^{234}U excess such that any
1017 measured $^{238}\text{U}/^{206}\text{Pb}$ dates will be inaccurate.

1018

1019 Cave drip-water that generates speleothem deposits typically has excess ^{234}U relative to
1020 secular equilibrium, although sometimes ^{234}U is depleted. Overall, most cave systems have
1021 initial activity ratios that are not grossly offset from secular equilibrium. This means that an



1022 uncertainty limit can be placed on such carbonates with reasonable confidence.
1023 Disequilibrium corrections will significantly affect age estimates with high precision, but not
1024 the low precision estimates that typically characterise LA-ICP-MS dates. For example,
1025 Woodhead et al. (2019) used an estimate of 1.0 ± 0.3 for $^{234}\text{U}/^{238}\text{U}_0$ in their study of
1026 speleothems from the Nullarbor plain, Australia, and this had negligible impact on the
1027 resultant compilation of U-Pb dates. Hopley et al. (2019) estimated a range of $^{234}\text{U}/^{238}\text{U}_0 =$
1028 1.26 to 2.99 for the 'Cradle of Humankind' in South Africa, with a mean of 1.9, and
1029 discussed a resulting potential age range of 5.8 to 4.8 Ma. A known excursion from 'typical'
1030 activity ratios is the Transvaal Dolomite Aquifer, also in South Africa. Speleothem deposits
1031 in cave systems that interacted with water from this aquifer have anomalously high U
1032 activity ratios ranging from ca. 2 to 12 (Kronfeld et al., 1994). This well-known occurrence
1033 highlights that speleothem deposits could arise from fluids with variable and anomalous
1034 activity ratios, and thus that attention must be given to accurately estimating the $^{234}\text{U}/^{238}\text{U}_0$
1035 when dating such deposits.
1036
1037 Unfortunately, activity ratio data that is relevant to hydrothermal and other vein-filling
1038 carbonates is sparse and potentially more variable. Carbonates precipitated in the shallow
1039 crust may arise from percolating groundwater, seawater, deep brines, formation waters, or
1040 a mixture of these sources. We can use existing data on these fluid sources to make an
1041 initial estimate of what range may exist in terrestrial carbonates. Groundwater is well known
1042 to have highly variable and significant ^{234}U excess (e.g. Osmond and Cowart, 1976). Figure
1043 16 shows a compilation of $^{234}\text{U}/^{238}\text{U}$ activity ratios taken from a range of literature sources
1044 (see supplementary file for sources). The population of data for groundwater (Figure 16A),
1045 mostly shallow, but including some saline and deeper samples, has a median activity ratio
1046 of 2.25, and is skewed towards higher values, with a significant tail up to ~11. Data from
1047 hydrothermal fluids and deep brines are less abundant in the literature, but can be
1048 estimated from young carbonates precipitated in travertines and hydrothermal veins. The
1049 compilation shown in Figure 16B is skewed towards samples from Turkey and surrounding
1050 regions. It has a median of 1.41, and is right-skewed with a tail ranging up to ~8 and only a
1051 few higher values.
1052



1053

1054

1055 *Figure 16. Compilation of uranium $^{234}\text{U}/^{238}\text{U}$ activity ratios from the literature of: A)*
1056 *groundwater and deep brines - these are present-day $^{234}\text{U}/^{238}\text{U}$ values (note the compilation*
1057 *is dominated by shallow groundwater rather than brines); and B) travertines and calcite*
1058 *precipitated in veins, commonly but not exclusively associated with travertines – these are*
1059 *estimated $^{234}\text{U}/^{238}\text{U}_0$ values.*

1060

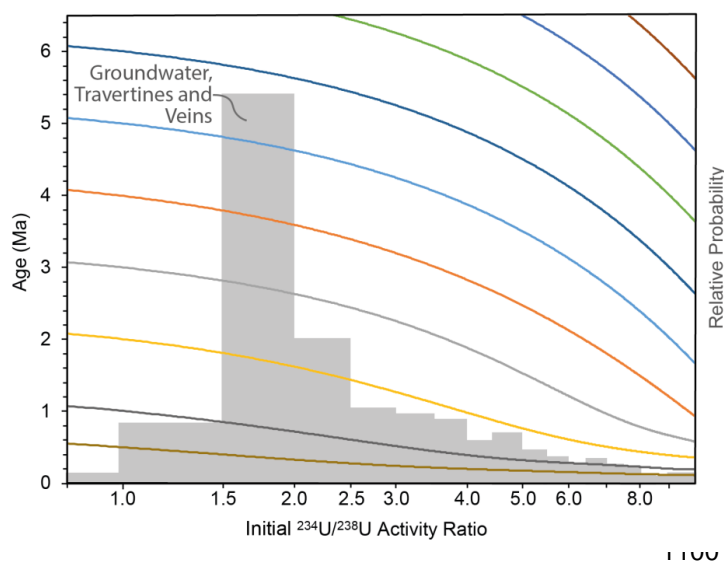
1061

1062 The compilations in Figure 16 are somewhat alarming, as they suggest that activity ratios
1063 have a high likelihood of being secular equilibrium ($^{234}\text{U}/^{238}\text{U}$ of ~ 1) in vein-filling
1064 carbonates. The compilations shown are biased by sampling, so uncertainties on the range
1065 of activity ratios should not be based on these compilations. However, a very conservative
1066 view would be that shallow groundwater $^{234}\text{U}/^{238}\text{U}$ activity ratios average closer to ~ 2 than
1067 they do to ~ 1 ; hydrothermal waters average closer to ~ 1.5 ; and permissible values may be
1068 extremely out of secular equilibrium at >10 . The data reveal that precise age estimates of
1069 young carbonates derived from crustal fluids are going to be severely hampered by a lack
1070 of knowledge of the U activity ratios.

1071



1072 To demonstrate the effect of initial activity ratios out of secular equilibrium, we have
1073 modelled synthetic data in Figure 17. This figure shows curves representing samples of ten
1074 different ages, which would range from 500 ka to 9 Ma if $^{234}\text{U}/^{238}\text{U}_0$ was in secular
1075 equilibrium (~ 1) during formation. The true age of the samples get younger as $^{234}\text{U}/^{238}\text{U}_0$
1076 increases. The effect does not decrease in significance as we look at older ages, i.e. the
1077 age offset on a sample with a measured age of 8 Ma is similar to that on a sample of 4 Ma.
1078 The curves are shown on a log scale, because in many systems, the variation in activity
1079 ratio is going to vary a small amount, close to secular equilibrium (~ 1). For example, in the
1080 Nullarbor plain cave systems, the variation is likely to be within 30% of 1 (Woodhead et al.,
1081 2019). Systems with large variations in initial activity ratios, for example some hydrothermal
1082 systems, would lead to a large uncertainty on the obtained dates. Ignoring the effect of the
1083 likely ^{234}U excess in vein-filling carbonates is likely to lead to significant inaccuracy of dates
1084 by 10s of %, in general by overestimating the age. Considering the impact that
1085 unconstrained initial $^{234}\text{U}/^{238}\text{U}$ ratios have on young dates leads to significant ($> 10\%$)
1086 uncertainties.
1087



1101 *Figure 17. Curves in different colours showing how an individual $^{206}\text{Pb}/^{238}\text{U}$ age (y-axis) will*
1102 *vary with a change in the initial $^{234}\text{U}/^{238}\text{U}$ activity ratio (x-axis). For example, a sample*
1103 *providing a measured $^{206}\text{Pb}/^{238}\text{U}$ age of 5 Ma will actually have a true age of 3.1 Ma if the*
1104 *initial $^{234}\text{U}/^{238}\text{U}$ is as high as 6. The grey histogram shows the combined compilations of*
1105 *groundwater, travertine and vein data from Figure 16.*



1106

1107

1108 So far, the discussion has involved the uncertainties surrounding excess/deficient ^{234}U
1109 during calcite growth. However, there are several other intermediate daughter products in
1110 the uranium decay chains that can pose problems for the accuracy of measured ages; see
1111 Richards et al. (1998) and Woodhead et al. (2006) for previous discussion of these. The
1112 isotope ^{230}Th is a potential consideration in the accuracy of ^{238}U - ^{206}Pb ages. In general,
1113 most speleothem-dating studies assume no initial ^{230}Th in the system, as Th is very
1114 insoluble in water compared to U. Any excess initial ^{230}Th during formation would also result
1115 in artificially old measured ages. ^{231}Pa is another daughter product in the decay chain,
1116 which again, is considered very insoluble, and does not form part of the disequilibrium
1117 corrections at present. ^{226}Ra , another intermediate product, may co-precipitate with U, but
1118 its short half-life of 1.6 ka means it is likely to have little impact on U-Pb ages (Richards et
1119 al., 1998). A final concern is the gas ^{222}Rn , as this may be lost from the system by diffusive
1120 processes. A study into the effect of this showed negligible impact on the ^{238}U - ^{206}Pb ages of
1121 a Quaternary speleothem (Richards et al., 1998).

1122

1123 Although the effects of disequilibrium in these shorter-lived intermediate daughter products
1124 is considered to be minor, and likely within the uncertainty of measured LA-ICP-MS U-Pb
1125 dates, it is worth noting that hydrological systems outside of those concerning speleothems
1126 and meteoric water have not been explored. Most of the issues presented here, particularly
1127 the excess ^{234}U problem, are part of the ^{238}U decay chain, and thus have implications for
1128 $^{238}\text{U}/^{206}\text{Pb}$ and lower intercept ages. The ^{235}U decay chain has different intermediate
1129 daughter products, and thus measured $^{235}\text{U}/^{207}\text{Pb}$ and lower intercept ages will be affected
1130 by a different set of processes. The problem of excess ^{234}U is alleviated if ^{235}U - ^{207}Pb ages
1131 can be used instead of ^{238}U - ^{206}Pb ages. However, there have been few attempts to utilise
1132 ^{235}U - ^{207}Pb dates (e.g. Hopley et al., 2019) because the low abundances of these isotopes in
1133 comparison to ^{238}U and ^{206}Pb are major limitations on the uncertainty of the measurements.
1134 Engel et al. (2019) have provided a solution that will potentially increase the accuracy of
1135 age estimates for speleothems, utilising the ^{235}U decay chain, as well as using ^{208}Pb in
1136 place of ^{204}Pb as the initial lead composition. This approach is based on ID, and it is unclear
1137 how effective it will be for LA-ICP-MS dating, given that ^{204}Pb is difficult to measure at high
1138 precision.

1139



1140 In summary, initial disequilibrium is clearly a major issue for the accuracy of U-Pb dating of
1141 carbonates. The effect is significant for material of any age, but as we get to older
1142 carbonates, the analytical uncertainty contributions will begin to swamp the uncertainties
1143 surrounding disequilibrium. For dating of Neogene-Quaternary carbonates, prior knowledge
1144 of likely activity ratios (e.g. by measuring younger or present-day values of the precipitating
1145 fluid, and inferring no change back in time) is critical for precise and accurate dates. The
1146 variation in hydrothermal systems that mix meteoric water with older brines is likely to be
1147 large in terms of the degree of ^{234}U excess. More information is needed to further
1148 understand what sort of values can be expected in different systems and different settings.
1149 From our preliminary compilation, it is apparent that ^{234}U excess is the norm, rather than the
1150 exception. For now, the absolute values and uncertainties on young dates (late Neogene to
1151 Quaternary) with no estimation of the initial disequilibria should be treated with caution.

1152

1153 **10. Dating old material – dealing with a potentially open system**

1154 Many early carbonate dating studies were attempted on very old material, i.e. Proterozoic
1155 and Archaean (e.g. Moorbath et al., 1987; Jahn, 1998; Taylor and Kalsbeek, 1990;
1156 Whitehouse and Russell, 1997); these mostly utilised Pb-Pb dating. A major issue of the
1157 Pb-Pb method, is that Pb contents of crustal fluids are much higher than that of the primary
1158 carbonates, and therefore, even small amounts of fluid-related alteration can dominate the
1159 measured Pb-Pb composition and lead to an age that is not representative of primary
1160 carbonate precipitation (e.g. Sumner & Bowring, 1996). Although there have been a handful
1161 of studies dating old carbonate material since the 1990s (e.g. Ray et al., 2003; Sarangi et
1162 al., 2004; Babinski et al., 2007; Fairey et al., 2013), Pb-Pb and U-Pb dating of Precambrian
1163 material have become rarely used techniques. This is presumably due to the difficulty in
1164 obtaining meaningful primary ages of old material. The dominant reason for this difficulty
1165 can generally be distilled down to open-system behaviour, i.e. dating material that has
1166 remained a closed isotopic system since its formation is increasingly difficult with
1167 increasingly older material. This is simply because thermal- and/or fluid-induced mobility of
1168 parent and daughter isotopes becomes increasingly likely if the material has been exposed
1169 to multiple deformation-, burial-, uplift-, glaciation-, weathering- or fracture-related events.

1170

1171 Early studies documented various transformative processes and their impact on Pb-Pb/U-
1172 Pb isotope systematics, e.g. fluid infiltration in limestone (Smith et al., 1991), diagenetic



1173 change from aragonite to calcite (Jones et al., 1995), and resetting of Pb isotope signatures
1174 during metamorphism (Russell et al., 1996; Whitehouse and Russell, 1997; Babinski et al.,
1175 1999). In general, the existence of some form of open-system behaviour within a given
1176 dataset has only been recognised through the isotopic data themselves, not through an
1177 independent dataset. This is simply achieved by assessing the robustness of the Pb-Pb or
1178 U-Pb data array with mathematical means, e.g. using the MSWD value, and explaining
1179 analytical scatter outside of a robust array as due to open system behaviour. With *in situ*
1180 methods, the approaches that we have described in Section 5 may allow for some
1181 independent removal of data that pertains to open-system behaviour, leaving a dataset that
1182 corresponds to a closed system.

1183

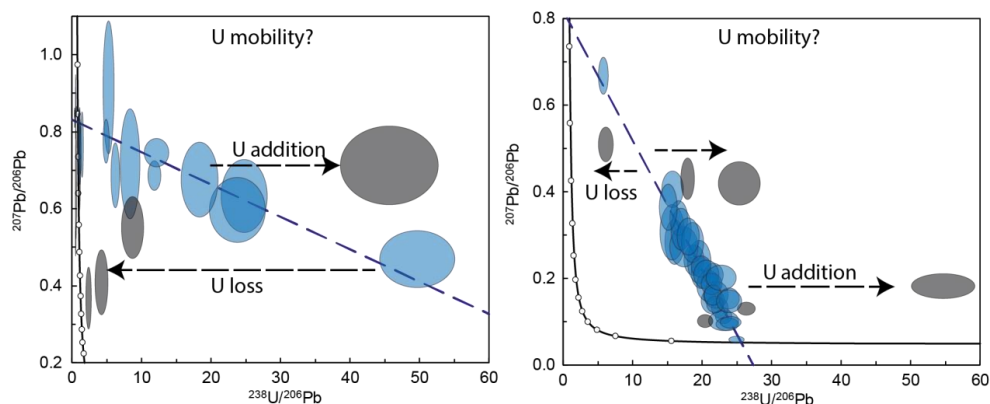
1184 A method that has been utilised to screen for altered samples in whole-rock geochemistry,
1185 is to test for effects of modern weathering using $^{234}\text{U}/^{238}\text{U}$ ratios (Albut et al., 2019). Ancient
1186 samples should have measured $^{234}\text{U}/^{238}\text{U}$ activity ratios in secular equilibrium, and
1187 departure from this in a measured sample would imply a more recent addition or subtraction
1188 of ^{234}U through weathering processes, indicating some modern fluid-rock interaction. This
1189 method of sample screening has not been applied to U-Pb dating, but we suggest is worthy
1190 of investigation.

1191

1192 In Figure 5 we documented various U-Pb datasets to demonstrate the range of behaviour
1193 that is seen with natural carbonates. Here we provide some additional comments regarding
1194 open-system behaviour, first in terms of U mobility, followed by that of Pb mobility. Uranium
1195 is mobile in oxidising fluids, so U enrichment and depletion relative to Pb is assumed to be
1196 the most common cause of open-system behaviour that will occur in natural carbonates. In
1197 Tera-Wasserburg space ($^{238}\text{U}/^{206}\text{Pb}$ vs. $^{207}\text{Pb}/^{206}\text{Pb}$), U mobility will be apparent as sub-
1198 horizontal trends in the data, with movement to the right reflecting gain of ^{238}U , and
1199 movement to the left reflecting loss of ^{238}U (see Figure 18). During a period of mobility,
1200 uranium may move into a fluid-phase, such that the remaining carbonate solid remains
1201 variably depleted in ^{238}U , or, uranium may partially move from its original location to another
1202 within the measured sample volume. In the former, this can sometimes be detected from
1203 the isotopic data if a distinct departure from a robust regression is defined by a sub-
1204 horizontal array (see Figures 5d and 18). In the latter case of uranium mobility, some
1205 domains will be depleted, whereas others will be enriched. This may be difficult to ascertain
1206 from the isotopic data alone if the mobility is pervasive through the material, because the



1207 induced scatter in the U-Pb regression (from both positive and negative movement in
1208 $^{238}\text{U}/^{206}\text{Pb}$) cannot be resolved from other causes of scatter, such as mixing between
1209 different age domains.
1210



1211
1212 *Figure 18. Tera-Wasserburg plots for LA-ICP-MS U-Pb data from two slicken-fibre calcite*
1213 *samples that exhibit potential open system behaviour caused by U mobility. Vectors for U*
1214 *loss and gain are schematic. Evidence for such U mobilisation requires additional lines of*
1215 *evidence that are currently lacking.*

1216
1217 Lead can substitute for Ca in the calcite lattice, and is also insoluble in most upper crustal
1218 fluids, for these reasons, U mobility is generally considered in favour of Pb mobility. Fluid-
1219 assisted mobility of U is certainly the most likely cause of open system behaviour because
1220 of the solubility of some U species. However, at high temperatures, solid-state diffusion is
1221 also a factor of consideration. Based on experimental data, Pb diffusion in calcite is
1222 essentially slow enough to be non-existent below 300°C (when considering the composition
1223 of a grain 1 mm in diameter; Cherniak, 1997); however, at higher temperatures (>400°C),
1224 diffusion of lead is possible if encountered for long periods (> 20 Myrs). Empirical
1225 observations of Pb (or U) diffusion in calcite are lacking. Diffusion is unlikely in the low
1226 temperature calcites that have formed the basis of most modern LA-ICP-MS dating studies;
1227 however, carbonates form in a range of higher temperature environments as well, such as
1228 alteration veins within deeply subducted crust. Understanding how the calcite U-Pb system
1229 works at medium to high-metamorphic grades may therefore become very relevant
1230 information, allowing this chronometer to be used to understand dates and rates in deep
1231 crustal environments.



1232

1233

1234 **11. Discussion**

1235 LA-ICP-MS U-Pb carbonate geochronology has been demonstrated by this and previous
1236 studies, to offer a potentially robust technique to date the timing of carbonate mineral
1237 formation. Limitations on the technique arise from several challenges. These include the
1238 typically low U content of carbonates in many settings, the propensity for carbonate to
1239 include significant concentrations of Pb upon formation, and the ease with which fluids can
1240 alter or reprecipitate mineral growth. LA-ICP-MS is an *in situ* technique, with high spatial
1241 resolution compared to physical sampling for bulk dissolution studies, which enables many
1242 of the hurdles in carbonate geochronology to be overcome. Rare and localised high U
1243 domains can be located and sampled, a range of U/Pb ratios can be targeted to generate a
1244 spread in isochron regressions, and altered domains, inclusions and secondary
1245 mineralisation can often be avoided.

1246

1247 Accurate and informative U-Pb carbonate geochronology demands careful imaging and
1248 petrographic analysis to establish a link between date and process. Various imaging
1249 techniques can be utilised prior to or after dating to aid with mineral characterisation, and
1250 with refinement and interpretation of the resulting age data. We refer to this as image-
1251 guided analysis. An alternative technique involves directly determining age data from
1252 image-based data itself, which we refer to as image-based analysis. Both techniques have
1253 their different benefits and applicability, and their efficacy depends on the instrumentation
1254 used and the type of material; for example, quadrupole ICP-MS is suited to image-based
1255 analysis, as a large element suite can be measured. Limitations on using quadrupole
1256 instrumentation are the detection limits for U and Pb when counting a large suite of
1257 elements. In contrast, multi-collector instruments can be used for image-based analysis,
1258 and have a very low detection limit, but the mass range is restricted between Hg and U,
1259 meaning that additional elements useful for understanding the U and Pb distribution cannot
1260 be measured simultaneously. Overall, image-based analysis is only nascent in
1261 geochronology, and as such has not been fully explored.

1262



1263 11.1. Limitations

1264 There are several limitations to LA-ICP-MS U-Pb carbonate geochronology. The
1265 heterogeneous nature of carbonate materials pose a problem that is difficult to circumvent.
1266 The relatively high spatial resolution of laser ablation already offers the best solution to this
1267 problem, but detection limits and the very low U and Pb contents mean that spots >150 μm
1268 are commonly employed, hampering the full ability of laser ablation to target fine-scale (<
1269 50 μm) zonation. Improvements in efficiency of ICP-MS instrumentation and of the ablation
1270 process are possible solutions to his issue.

1271

1272 At present, there is only one reference material in circulation that has been widely used and
1273 documented for the purpose of U-Pb normalisation (WC-1; Roberts et al., 2017). WC-1 has
1274 an uncertainty on its U/Pb ratio of 2.5% 2σ . Using this material for normalisation of U/Pb
1275 ratios, or for validation of the method accuracy, limits the final age uncertainty of any
1276 particular sample to \sim 2.5%. To improve beyond this range requires the characterisation of
1277 natural (or production and characterisation of U and Pb doped synthetic) materials, with a
1278 final U/Pb precision better than 2.5%. There is also a requirement for additional well
1279 characterised materials (i.e. those with robust U-Pb systematics and well documented ID U-
1280 Pb datasets) that can be used as secondary reference materials (i.e. those run as
1281 unknowns), for assessment of accuracy and long-term reproducibility.

1282

1283 Another major limitation is the nature of carbonate matrices, and the lack of quantified data
1284 on the matrix effect between different carbonate minerals and structures. Inter-element
1285 fractionation (i.e. U/Pb in this case) is one of the major limitations on the reproducibility and
1286 accuracy of laser ablation U-Pb dating. For this reason, matching matrices of the reference
1287 material with that of the sample has been standard practise in U-bearing accessory mineral
1288 geochronology. Several groups have tried to limit the effect of this issue by utilising
1289 normalisation and date reduction procedures that reduce the effect (e.g. Burn et al., 2017;
1290 Neymark et al., 2018), but regardless of the matrix used for normalisation, validation of the
1291 method should still utilise a similar matrix to the sample. Carbonates clearly have a large
1292 range of structures, even with calcite, for example, sparry to micritic, with wide-ranging
1293 crystal/grain-sizes and porosity. Nuriel et al. (2019) noted differences between the use of
1294 coarse-grained sparry reference materials to fine-grained polycrystalline reference
1295 materials, with the latter being skewed towards older ages by several percent. To move



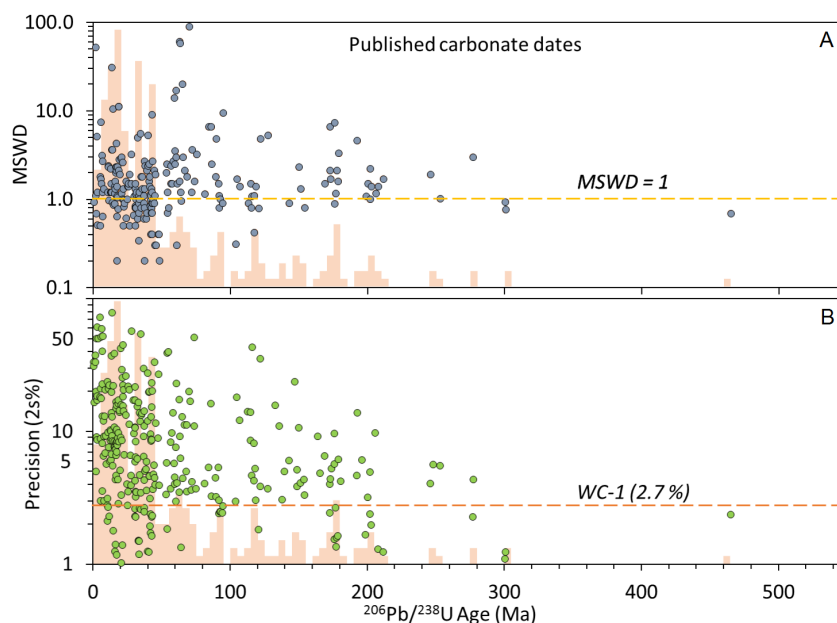
1296 towards better precision and accuracy of the LA-ICP-MS U-Pb method, it will be necessary
1297 to have a range of well characterised reference materials that cover variable carbonate
1298 mineralogy (e.g. aragonite, dolomite, calcite), as well as internal morphology and texture.
1299

1300 11.2. Applications

1301 To date, LA-ICP-MS U-Pb carbonate geochronology has been applied to a wide range of
1302 applications. These include the dating of speleothem deposition (Hopley et al., 2019;
1303 Scardia et al., 2019), brittle deformation (Roberts & Walker, 2016; Ring & Gerdes, 2016;
1304 Goodfellow et al., 2017; Hansman et al., 2018; Parrish et al., 2018; Beaudoin et al., 2018;
1305 Nuriel et al., 2017, 2019; Smeraglia et al., 2019), hydrocarbon migration (Holdsworth et al.,
1306 2019), hydrothermal ore mineralisation (Burisch et al., 2017, 2019), hydrothermal fluid flow
1307 (Mazurek et al., 2018; Walter et al., 2018; Incerpi et al., 2019; MacDonald et al., 2019);
1308 pedogenesis (Methner et al., 2016; Liivamägi et al., 2019); ocean crust alteration (Coogan
1309 et al., 2016), diagenesis in sedimentary deposits (Li et al., 2014; Pagel et al., 2018;
1310 Mangenot et al., 2018; Godeau et al., 2018; Lawson et al., 2018) and sedimentary
1311 deposition (Drost et al., 2018). Published dates range in age from 0.6 to 548 Ma (see
1312 Figure 19), MSWDs range from 0.2 to 89 (Figure 19a), and quoted uncertainties range from
1313 0.6 to 143 % (2 σ ; Figure 19B). The majority of dated samples so far range from the
1314 Neogene to Jurassic, with ~50% being Oligocene or younger. Across this age range, the
1315 uncertainty is variable and uncorrelated to age or MSWD, demonstrating that the age
1316 uncertainty reflects an interplay of factors, and includes the heterogeneous nature of
1317 carbonate materials. It should be noted however, that many dates with large uncertainties
1318 or mixed results are likely unpublished, biasing this compilation towards successful
1319 samples. For example, it is possible that many unreported and failed attempts at dating
1320 samples that are Palaeozoic and older have been made.

1321

1322



1323

1324

1325 *Figure 19. Compilation of published LA-ICP-MS U-Pb dates of carbonate (n=318). A)*

1326 *MSWD plotted against $^{206}\text{Pb}/^{238}\text{U}$ age; and B) Precision as 2s % plotted against $^{206}\text{Pb}/^{238}\text{U}$*

1327 *age. The histograms in the background show the distribution of dates.*

1328

1329 A major benefit of carbonate geochronology is that carbonate minerals record an archive of
1330 data that can be linked to the age of formation. Fluid inclusions, stable isotopes (carbon and
1331 oxygen), radiogenic isotopes (strontium), and elemental compositions all reveal insight into
1332 the fluid composition that precipitated the mineral. This combination has long been an
1333 approach within the field of palaeohydrology; however, the timing of mineralisation and
1334 hence fluid-flow has generally involved only relative estimates with large uncertainties, or
1335 the dating of phases associated with higher-temperature activity (e.g., Re-Os dating of
1336 Molybdenite). The addition of absolute chronological information is a critical step to
1337 understand the timing of fluid-flow through the crust in a range of settings, for example,
1338 within hydrocarbon-bearing basins, within ore-forming mineral systems, and within upper
1339 crustal bedrock that may be used to host anthropogenic waste/outputs (e.g. radioactive
1340 waste, storage and sequestration of CO_2).

1341



1342 A benefit of utilising LA-ICP-MS as a method of dating, is that the same crystals that have
1343 been dated can be measured for various other chemical proxies and signatures. Several
1344 previous studies have combined fluid inclusions and/or stable carbon and oxygen isotope
1345 analysis with LA-ICP-MS dating (e.g. Mangenot et al., 2018; Pagel et al., 2018; Goodfellow
1346 et al., 2016; Walter et al., 2018), but for most of these, it is not clear if the same volume of
1347 material, or simply the same genetic domain has been sub-sampled for both the dating as
1348 well the additional isotope analyses. Use of petrography and imaging allows for the same
1349 genetic domain to be analysed for several methods; however, there are also several
1350 approaches that allow for an overlapping analytical volume to be analysed. Dated material
1351 can be micro-drilled or -milled following laser ablation, with the powder being analysed for
1352 additional chemical information (e.g. Sr, C, O isotopes). Alternatively, thin sections or
1353 polished blocks can be analysed using a combination of in situ techniques, for example, ion
1354 microprobe measurement of stable isotope and/or elemental compositions, and laser
1355 ablation measurement of Sr isotopes, elemental compositions along with U-Pb dating.
1356 Drake et al. (2017) demonstrated the utility of combining ion microprobe stable carbon and
1357 oxygen isotope analysis with U-Pb dating to study palaeohydrology and ancient microbial
1358 activity.

1359
1360 In addition to traditional carbon and oxygen isotope measurements ($\delta^{13}\text{C}$ and $\delta^{18}\text{O}$),
1361 clumped isotopes ($\Delta 47$) can provide the temperature of mineral formation (e.g. Eiler, 2007).
1362 Several studies have demonstrated the combination of clumped isotope thermometry with
1363 dating (e.g. Quade et al., 2018; Mangenot et al., 2018; Lawson et al., 2017; MacDonald et
1364 al., 2019). These apply the technique to the dating of paleosols for climatic records,
1365 diagenetic mineralisation for basin histories, and hydrothermal veins to understand crustal
1366 fluid-flow. This combination of techniques is a clear growth area with a range of applications
1367 across earth and environmental science.

1368
1369 Finally, carbonates also comprise a host of major and trace metals that offer further isotopic
1370 information that has yet to be fully explored, for example, stable isotopes of Ca, Zn, Fe, and
1371 Cu. Linking these with U-Pb dates from the same material could provide high resolution
1372 records of natural fractionation processes in subsurface environments.

1373



1374 **12. Conclusions**

1375 We have demonstrated the heterogeneous nature of carbonate minerals, in terms of U and
1376 Pb distribution and isotopic systematics. Although we have focused on vein-filling calcite,
1377 most of the issues highlighted in this paper are relevant to other carbonate dating
1378 applications. Various imaging techniques can be used to screen material, and to
1379 characterise U-Pb heterogeneity; a combination of these techniques is crucial to
1380 understand what exactly has been dated. Linking age information to spatial data, imagery
1381 or elemental maps, is crucial to understanding heterogeneous isotopic data. Two main
1382 approaches to dating have been presented, the traditional approach of static spot ablations
1383 guided by independent image data, and an alternative approach of age mapping using
1384 software analysis of 2D isotopic map data. Each of these approaches have benefits and
1385 drawbacks, and the choice between them will partly be governed by the instrumentation
1386 available. The applications of carbonate U-Pb geochronology are vast, with a key benefit to
1387 the laser ablation approach being that specific volumes of material can be analysed for
1388 several isotopic and elemental proxies and signatures, whilst also providing absolute
1389 chronological information. The LA-ICP-MS method is limited by factors that include the
1390 uncertainties on reference material isotope ratios, matrix effects and long-term
1391 reproducibility; taking these into consideration, the method is best applied to applications
1392 where age uncertainties of greater than 3-4% are of benefit. For applications where high
1393 precision (i.e. <1%) is required, such as calibration of palaeoclimate records or of
1394 evolutionary change, then follow-up analysis with ID is the only method that can potentially
1395 achieve the necessary precision. The future of the method in terms of accuracy and
1396 precision requires well characterised (by Isotope Dilution methods) reference materials
1397 covering a range of carbonate matrices. The range of studies published over the last five
1398 years (2014 to 2019) have revealed a wide array of geoscience applications that are both
1399 amenable to, and benefit from, LA-ICP-MS U-Pb carbonate geochronology.

1400

1401 **13. Acknowledgements**

1402 The authors acknowledge the Natural Environment Research Council for National
1403 Capability funding of the National Environment Isotope Facility. N Roberts, D Condon, M
1404 Horstwood, A Milodowski and R Haslam publish with the permission of the Executive
1405 Director of the British Geological Survey. D Chew and K Drost acknowledge a Science
1406 Foundation Ireland grant (15/IA/3024) that is partly funded by the Geological Survey of



1407 Ireland and the Environmental Protection Agency, Ireland. HD acknowledges Swedish
1408 Research Council grant (2017-05186) and Formas grant (2017-00766).

1409

1410

1411

1412 **14. Appendix**

1413 14.1. Implications of age data

1414 The focus of this paper is not on the meaning of the age data presented, or its implications
1415 for faulting or fluid-flow; however, we provide brief information for interested readers.

1416

1417 14.2. Example A and D - Variscan-related veins in the Northumberland Basin

1418 The age of ca. 287 Ma for the dated calcite crystal can be linked to deformation of the host
1419 rock based on the vein structure. The calcite is taken from a planar fracture forming on the
1420 axial plane of a small fold that has accommodated bedding-plane sliding (Fig. 8). The
1421 fracture is filled with calcite mineralisation of the stretched vein type (Bons et al., 2012), and
1422 that is interpreted to have formed soon after opening of the vein, and synchronous with
1423 deformation. The age of ca. 287 Ma broadly overlaps with the intrusion of the Whin Sill (ca.
1424 297 Ma; Heaman pers. comm. within De Paola et al., 2005), and is therefore compatible
1425 with the model of partitioned transpression of De Paola et al. (2005), who suggest that
1426 deformation was synchronous with the Whin Sill intrusion.

1427

1428 14.3. Example B - Faroe Island brittle faults

1429 The significance of the Eocene ages has been discussed by Roberts & Walker (2016). This
1430 paper was the first to demonstrate the applicability of LA-ICP-MS U-Pb carbonate
1431 geochronology to dating brittle structures in the upper crust.

1432

1433 14.4. Example C - Sellafield fracture mineralisation

1434 Sample 877 was collected from the modern-day saline transition zone between the upper
1435 fresh groundwater system and the deeper saline basinal-basement groundwater system, at
1436 a depth of -635 m OD within the St Bees Sandstone Group (Triassic) in Sellafield borehole
1437 BH10A (equivalent to sample B697 and D750: Appendix Table S2, Milodowski et al., 2018).
1438 Externally, this calcite exhibits a “nailhead” (i.e. c-axis flattened) crystal habit (Figure 10).
1439 However, detailed petrographic analysis reveals it has a complex growth history:



1440 comprising of cores of c-axis-elongated calcite characteristic of the deeper saline
1441 groundwater that are syntaxially-overgrown by later equant and c-axis flattened calcite
1442 characteristic of the overlying fresh groundwater zone (Milodowski et al., 2018). The U-Pb
1443 analyses all come from within the saline groundwater zone type calcite core region (rather
1444 than the later freshwater-type overgrowth that has extremely low U).

1445
1446 Late-stage (generation “ME9”) calcite is a characteristic feature of the present-day fracture-
1447 controlled deep groundwater system in the Sellafield area of the west Cumbrian coastal
1448 plain (Milodowski et al., 2018). The resulting age suggests that ME9 calcite growth in the
1449 sampled fracture was initiated in the late Miocene, and has been preserved (or at least
1450 partially preserved until the present-day). The implication is that the modern groundwater
1451 system was developed following regional Miocene uplift and younger groundwater recharge
1452 relating to glaciations and/or uplift of the region, have not led to complete re-precipitation of
1453 fracture-filling calcite, with calcite precipitation continuing to the present-day. Taken
1454 together with other petrographic, stable isotope, strontium isotope, fluid inclusion,
1455 microchemical analyses and whole-crystal U-Th age dating, the age data support the
1456 interpretation that despite evidence for glacial recharge, the geochemical conditions (e.g.
1457 pH, Eh) have remained stable over this period at potential repository depths (cf. Milodowski
1458 et al., 2018).

1459

1460 14.5. Example E and F – Vein sets of the Bighorn Basin, Wyoming

1461 These samples are from vein sets in the sedimentary cover of the Bighorn Basin. These
1462 samples are part of a larger study that analysed the timing of deformation in the foreland of
1463 the Sevier and Laramide orogenies, and how this deformation propagated in time and
1464 space (Beaudoin et al., 2018). Sample BH11 is related to Laramide deformation, whereas
1465 sample BM18 is related to Sevier deformation.

1466

1467 14.6. Example G - Moab fault

1468 This sample comprises multiple thin (1 to 5 mm wide) veins collected from the footwall
1469 damage zone of the Moab Fault in southeast Utah. Regional deformation is primarily driven
1470 by salt tectonics (Gutierrez, 2004), and salt dissolution has produced up to one km of offset
1471 within the sedimentary rocks along the Moab Fault (Foxford et al., 1996). Fault zone
1472 deformation was closely associated with fluid flow and carbonate cementation (Eichhubl et



1473 al., 2009; Hodson et al., 2016). Ar-Ar ages from clay fault gauge range from 63 to 43 Ma
1474 and are interpreted to record the final episodes of faulting and fracture generation (Pevear
1475 et al., 1997; Solum et al., 2005). Our new lower intercept age of 22 Ma is imprecise, but
1476 clearly younger than the early-Tertiary ages. This suggests that circulating fluids continued
1477 to move along the fault zone long after the cessation of fault related deformation.

1478

1479 15. References

- 1480 1. Akhurst, M.C., Chadwick, R.A., Holliday, D.W., McCormac, M., McMillan, A.A.,
1481 Millward, D., Young, B., Ambrose, K., Auton, C.A., Barclay, W.J., Barnes, R.P.,
1482 Beddoe-Stephens, B., James, J.W.C., Johnson, H., Jones, N.S., Glover, B.W.,
1483 Hawkins, M.P., Kimberll, G.S., MacPherson, K.A.T., Merrit, J.W., Milodowski, A.E.,
1484 Riley, N.J., Robins, N.S., Stone, P. and Wingfield, R.T.R.: The geology of the west
1485 Cumbria district: Memoir of the British Geological Survey, Sheets 28, 37 and 47,
1486 British Geological Survey, Keyworth, UK, 1997
- 1487 2. Albut, G., Kamber, B.S., Brüske, A., Beukes, N.J., Smith, A.J. and Schoenberg, R.:
1488 Modern weathering in outcrop samples versus ancient paleoredox information in drill
1489 core samples from a Mesoarchaeon marine oxygen oasis in Pongola Supergroup,
1490 South Africa. *Geochimica et Cosmochimica Acta*, 265, 330-353, 2019.
- 1491 3. Babinski, M., Van Schmus, W.R. and Chemale Jr, F.: Pb–Pb dating and Pb isotope
1492 geochemistry of Neoproterozoic carbonate rocks from the São Francisco basin,
1493 Brazil: implications for the mobility of Pb isotopes during tectonism and
1494 metamorphism. *Chemical Geology*, 160, 175-199, 1999.
- 1495 4. Babinski, M., Vieira, L.C. and Trindade, R.I.: Direct dating of the Sete Lagoas cap
1496 carbonate (Bambuú Group, Brazil) and implications for the Neoproterozoic glacial
1497 events. *Terra Nova*, 19, 401-406, 2007.
- 1498 5. Baker, A.J., Lever, M.C., Thorne, M.C., Tweed, C.J., Wikramaratna, R.S.,
1499 Chambers, A.V., Fitzgerald, P.L., Ghabaee, K., Goodfield, M., Harris, A.W. and
1500 Haworth, A.: NIREX 97: an assessment of the post-closure performance of a deep
1501 waste repository at Sellafield, NIREX, UK, 1997.
- 1502 6. Baker, A., Smart, P.L., Barnes, W.L., Edwards, R.L. and Farrant, A.: The Hekla 3
1503 volcanic eruption recorded in a Scottish speleothem?. *The Holocene*, 5, 336-342,
1504 1995.



- 1505 7. Baker, A., Smith, C.L., Jex, C., Fairchild, I.J., Genty, D. and Fuller, L.: Annually
1506 laminated speleothems: a review. *International Journal of Speleology*, 37, 193-206,
1507 2008.
- 1508 8. Barnaby, R.J. and Rimstidt, J.D.: Redox conditions of calcite cementation interpreted
1509 from Mn and Fe contents of authigenic calcites. *GSA Bulletin*, 101, 795-804, 1989.
- 1510 9. Bath, A., Richards, H., Metcalfe, R., McCartney, R., Degnan, P. and Littleboy, A.:
1511 Geochemical indicators of deep groundwater movements at Sellafield, UK. *Journal*
1512 *of Geochemical Exploration*, 90, 24-44, 2006.
- 1513 10. Beaudoin, N., Lacombe, O., Roberts, N.M. and Koehn, D.: U-Pb dating of calcite
1514 veins reveals complex stress evolution and thrust sequence in the Bighorn Basin,
1515 Wyoming, USA. *Geology*, 46, 1015-1018, 2018.
- 1516 11. Bergman, S.C., Huntington, K.W. and Crider, J.G.: Tracing paleofluid sources using
1517 clumped isotope thermometry of diagenetic cements along the Moab Fault,
1518 Utah. *American Journal of Science*, 313, 490-515, 2013.
- 1519 12. Bertok, C., Barale, L., d'Atri, A., Martire, L., Piana, F., Rossetti, P. and Gerdes, A.,
1520 2019. Unusual marbles in a non-metamorphic succession of the SW Alps (Valdieri,
1521 Italy) due to early Oligocene hydrothermal flow. *International Journal of Earth*
1522 *Sciences*, 1-20, 2019.
- 1523 13. Bons, P.D., Elburg, M.A. and Gomez-Rivas, E.: A review of the formation of tectonic
1524 veins and their microstructures. *Journal of Structural Geology*, 43, 33-62, 2012.
- 1525 14. Brannon, J.C., Cole, S.C., Podosek, F.A., Ragan, V.M., Coveney, R.M., Wallace,
1526 M.W. and Bradley, A.J.: Th-Pb and U-Pb dating of ore-stage calcite and Paleozoic
1527 fluid flow. *Science*, 271, 491-493, 1996.
- 1528 15. Buckman, J.O., Corbett, P.W. and Mitchell, L.: Charge contrast imaging (CCI):
1529 revealing enhanced diagenetic features of a coquina limestone. *Journal of*
1530 *Sedimentary Research*, 86, 734-748, 2016.
- 1531 16. Burisch, M., Gerdes, A., Walter, B.F., Neumann, U., Fettel, M. and Markl, G.:
1532 Methane and the origin of five-element veins: mineralogy, age, fluid inclusion
1533 chemistry and ore forming processes in the Odenwald, SW Germany. *Ore Geology*
1534 *Reviews*, 81, 42-61, 2017.
- 1535 17. Burisch, M., Walter, B.F., Gerdes, A., Lanz, M. and Markl, G.: Late-stage anhydrite-
1536 gypsum-siderite-dolomite-calcite assemblages record the transition from a deep to a
1537 shallow hydrothermal system in the Schwarzwald mining district, SW
1538 Germany. *Geochimica et Cosmochimica Acta*, 223, 259-278, 2018.



- 1539 18. Burn, M., Lanari, P., Pettke, T. and Engi, M.: Non-matrix-matched standardisation in
1540 LA-ICP-MS analysis: general approach, and application to allanite Th–U–Pb
1541 dating. *Journal of analytical atomic spectrometry*, *32*, 1359-1377, 2017.
- 1542 19. Chan, M.A., Parry, W.T. and Bowman, J.R.: Diagenetic hematite and manganese
1543 oxides and fault-related fluid flow in Jurassic sandstones, southeastern Utah. *AAPG*
1544 *bulletin*, *84*, 1281-1310, 2000.
- 1545 20. Cherniak, D.J.: An experimental study of strontium and lead diffusion in calcite, and
1546 implications for carbonate diagenesis and metamorphism. *Geochimica et*
1547 *Cosmochimica Acta*, *61*, 4173-4179, 1997.
- 1548 21. Cole, J.M., Nienstedt, J., Spataro, G., Rasbury, E.T., Lanzirotti, A., Celestian, A.J.,
1549 Nilsson, M. and Hanson, G.N.: Phosphor imaging as a tool for in situ mapping of
1550 ppm levels of uranium and thorium in rocks and minerals. *Chemical Geology*, *193*,
1551 127-136, 2003.
- 1552 22. Cole, J.M., Rasbury, E.T., Hanson, G.N., Montañez, I.P. and Pedone, V.A.: Using U-
1553 Pb ages of Miocene tufa for correlation in a terrestrial succession, Barstow
1554 Formation, California. *Geological Society of America Bulletin*, *117*, 276-287, 2005.
- 1555 23. Coogan, L.A., Parrish, R.R. and Roberts, N.M.: Early hydrothermal carbon uptake by
1556 the upper oceanic crust: Insight from in situ U-Pb dating. *Geology*, *44*, 147-150,
1557 2016.
- 1558 24. Cuthbert, S.J. and Buckman, J.O.: Charge contrast imaging of fine-scale
1559 microstructure and compositional variation in garnet using the environmental
1560 scanning electron microscope. *American Mineralogist*, *90*, 701-707, 2005.
- 1561 25. Davatzes, N.C., Eichhubl, P. and Aydin, A.: Structural evolution of fault zones in
1562 sandstone by multiple deformation mechanisms: Moab fault, southeast
1563 Utah. *Geological Society of America Bulletin*, *117*, 135-148, 2005.
- 1564 26. De Paola, N., Holdsworth, R.E., McCaffrey, K.J. and Barchi, M.R.: Partitioned
1565 transtension: an alternative to basin inversion models. *Journal of Structural*
1566 *Geology*, *27*, 607-625, 2005.
- 1567 27. DeWolf, C.P. and Halliday, A.N.: U-Pb dating of a remagnetized Paleozoic
1568 limestone. *Geophysical Research Letters*, *18*, 1445-1448, 1991.
- 1569 28. Drake, H., Heim, C., Hoggmalm, K.J. and Hansen, B.T.: Fracture zone-scale variation
1570 of trace elements and stable isotopes in calcite in a crystalline rock setting. *Applied*
1571 *Geochemistry*, *40*, 11-24, 2014.



- 1572 29. Drake, H., Heim, C., Roberts, N.M.W., Zack, T., Tillberg, M., Broman, C., Ivarsson,
1573 M., Whitehouse, M.J. and Åström, M.E.: Isotopic evidence for microbial production
1574 and consumption of methane in the upper continental crust throughout the
1575 Phanerozoic eon. *Earth and Planetary Science Letters*, 470, 108-118, 2017.
- 1576 30. Drake, H., Mathurin, F.A., Zack, T., Schäfer, T., Roberts, N.M.W., Whitehouse, M.,
1577 Karlsson, A., Broman, C. and Åström, M.E.: Incorporation of metals into calcite in a
1578 deep anoxic granite aquifer. *Environmental science & technology*, 52, 493-502,
1579 2018.
- 1580 31. Drake, H., Tullborg, E.L., Hogmalm, K.J. and Åström, M.E.: Trace metal distribution
1581 and isotope variations in low-temperature calcite and groundwater in granitoid
1582 fractures down to 1 km depth. *Geochimica et Cosmochimica Acta*, 84, 217-238,
1583 2012.
- 1584 32. Drost, K., Chew, D., Petrus, J.A., Scholze, F., Woodhead, J.D., Schneider, J.W. and
1585 Harper, D.A.: An Image Mapping Approach to U-Pb LA-ICP-MS Carbonate Dating,
1586 and Applications to Direct Dating of Carbonate Sedimentation. *Geochemistry,*
1587 *Geophysics, Geosystems*, 19, 4631-4648, DOI:10.1029/2018GC007850, 2018.
- 1588 33. Eichhubl, P., Davatz, N.C. and Becker, S.P.: Structural and diagenetic control of fluid
1589 migration and cementation along the Moab fault, Utah. *AAPG bulletin*, 93, 653-681,
1590 2009.
- 1591 34. Eiler, J.M.: "Clumped-isotope" geochemistry—The study of naturally-occurring,
1592 multiply-substituted isotopologues. *Earth and planetary science letters*, 262, 309-
1593 327, 2007.
- 1594 35. Engel, J., Woodhead, J., Hellstrom, J., Maas, R., Drysdale, R. and Ford, D.:
1595 Corrections for initial isotopic disequilibrium in the speleothem U-Pb dating
1596 method. *Quaternary Geochronology*, 54, 101009, 2019.
- 1597 36. Engi, M., Lanari, P. and Kohn, M.J.: Significant ages—An introduction to
1598 petrochronology. *Reviews in Mineralogy and Geochemistry*, 83, 1-12, 2017.
- 1599 37. Fairey, B., Tsikos, H., Corfu, F. and Polteau, S.: U–Pb systematics in carbonates of
1600 the Postmasburg Group, Transvaal Supergroup, South Africa: primary versus
1601 metasomatic controls. *Precambrian Research*, 231, 194-205, 2013.
- 1602 38. Field, L.P., Milodowski, A.E., Evans, D., Palumbo-Roe, B., Hall, M.R., Marriott, A.L.,
1603 Barlow, T. and Devez, A.: Determining constraints imposed by salt fabrics on the
1604 morphology of solution-mined energy storage cavities, through dissolution



- 1605 experiments using brine and seawater in halite. *Quarterly Journal of Engineering*
1606 *Geology and Hydrogeology*, 52, 240-254, 2019.
- 1607 39. Flude, S., Lee, M.R., Sherlock, S.C. and Kelley, S.P.: Cryptic microtextures and
1608 geological histories of K-rich alkali feldspars revealed by charge contrast
1609 imaging. *Contributions to Mineralogy and Petrology*, 163, 983-994, 2012.
- 1610 40. Foxford, K.A., Garden, I.R., Guscott, S.C., Burley, S.D., Lewis, J.J.M., Walsh, J.J.
1611 and Watterson, J.: The field geology of the Moab fault, in: *Geology and Resources of*
1612 *the Paradox Basin*, Utah Geological Association, 25, 265-283, 1996.
- 1613 41. Godeau, N., Deschamps, P., Guihou, A., Leonide, P., Tendil, A., Gerdes, A.,
1614 Hamelin, B. and Girard, J.P.: U-Pb dating of calcite cement and diagenetic history in
1615 microporous carbonate reservoirs: Case of the Urganian Limestone,
1616 France. *Geology*, 46, 247-250, 2018.
- 1617 42. Goodfellow, B.W., Viola, G., Bingen, B., Nuriel, P. and Kylander-Clark, A.R.:
1618 Palaeocene faulting in SE Sweden from U–Pb dating of slickenfibres calcite. *Terra*
1619 *Nova*, 29, 321-328, 2017.
- 1620 43. Grandia, F., Asmerom, Y., Getty, S., Cardellach, E. and Canals, A.: U–Pb dating of
1621 MVT ore-stage calcite: implications for fluid flow in a Mesozoic extensional basin
1622 from Iberian Peninsula. *Journal of Geochemical Exploration*, 69, 377-380, 2000.
- 1623 44. Hansman, R.J., Albert, R., Gerdes, A. and Ring, U.: Absolute ages of multiple
1624 generations of brittle structures by U-Pb dating of calcite. *Geology*, 46, 207-210,
1625 2018.
- 1626 45. Hareyama, M., Tsuchiya, N., Takebe, M. and Chida, T.: Two dimensional
1627 measurement of natural radioactivity of granitic rocks by photostimulated
1628 luminescence technique. *Geochemical Journal*, 34, 1-9, 2000.
- 1629 46. Heathcote, J.A. and Michie, U.M.: Estimating hydrogeological conditions over the
1630 last 120 ka: an example from the Sellafield area, UK. *Journal of the Geological*
1631 *Society*, 161, 995-1008, 2004.
- 1632 47. Hellwig, A., Voigt, S., Mulch, A., Frisch, K., Bartenstein, A., Pross, J., Gerdes, A. and
1633 Voigt, T.: Late Oligocene to early Miocene humidity change recorded in terrestrial
1634 sequences in the Ili Basin (south-eastern Kazakhstan, Central
1635 Asia). *Sedimentology*, 65, 517-539, 2018.
- 1636 48. Hodson, K.R., Crider, J.G. and Huntington, K.W.: Temperature and composition of
1637 carbonate cements record early structural control on cementation in a nascent



- 1638 deformation band fault zone: Moab Fault, Utah, USA. *Tectonophysics*, 690, 240-252,
1639 2016.
- 1640 49. Holdsworth, R.E., McCaffrey, K.J.W., Dempsey, E., Roberts, N.M.W., Hardman, K.,
1641 Morton, A., Feely, M., Hunt, J., Conway, A. and Robertson, A.: Natural fracture
1642 propping and earthquake-induced oil migration in fractured basement
1643 reservoirs. *Geology*, in press, [DOI:10.1130/G46280.1](https://doi.org/10.1130/G46280.1), 2019.
- 1644 50. Hopley, P.J., Reade, H., Parrish, R., De Kock, M. and Adams, J.W.: Speleothem
1645 evidence for C3 dominated vegetation during the Late Miocene (Messinian) of South
1646 Africa. *Review of Palaeobotany and Palynology*, 264, 75-89, 2019.
- 1647 51. Horstwood, M.S.A., Košler, J., Gehrels, G., Jackson, S.E., McLean, N.M., Paton, C.,
1648 Pearson, N.J., Sircombe, K., Sylvester, P., Vermeesch, P. and Bowring, J.F.:
1649 Community-derived standards for LA-ICP-MS U-(Th-) Pb geochronology—Uncertainty
1650 propagation, age interpretation and data reporting. *Geostandards and Geoanalytical
1651 Research*, 40, 311-332, 2016.
- 1652 52. Incerpi, N., Martire, L., Manatschal, G., Bernasconi, S.M., Gerdes, A., Czuppon, G.,
1653 Palcsu, L., Karner, G.D., Johnson, C.A. and Figueredo, P.H.: Hydrothermal fluid flow
1654 associated to the extensional evolution of the Adriatic rifted margin: Insights from the
1655 pre-to post-rift sedimentary sequence (SE Switzerland, N ITALY). *Basin Research*, in
1656 press, DOI:10.1111/bre.12370, 2019.
- 1657 53. Jahn, B.M.: Pb–Pb dating of young marbles from Taiwan. *Nature*, 332, 429, 1988.
- 1658 54. Jahn, B.M. and Cuvellier, H.: Pb–Pb and U–Pb geochronology of carbonate rocks: an
1659 assessment. *Chemical Geology*, 115, 125-151, 1994.
- 1660 55. Johansen, T.E.S., Fossen, H. and Kluge, R.: The impact of syn-faulting porosity
1661 reduction on damage zone architecture in porous sandstone: an outcrop example
1662 from the Moab Fault, Utah. *Journal of Structural Geology*, 27, 1469-1485, 2005.
- 1663 56. Jones, C.E., Halliday, A.N. and Lohmann, K.C.: The impact of diagenesis on high-
1664 precision U–Pb dating of ancient carbonates: An example from the Late Permian of
1665 New Mexico. *Earth and Planetary Science Letters*, 134, 409-423, 1995.
- 1666 57. Kelly, S.D., Newville, M.G., Cheng, L., Kemner, K.M., Sutton, S.R., Fenter, P.,
1667 Sturchio, N.C. and Spötl, C.: Uranyl incorporation in natural calcite. *Environmental
1668 Science & Technology*, 37, 1284-1287, 2003.
- 1669 58. Kreissl, S., Gerdes, A., Walter, B.F., Neumann, U., Wenzel, T., Markl, G.:
1670 Reconstruction of a >200 Ma multi-stage “five element” Bi–Co–Ni–Fe–As–S system in
1671 the Penninic Alps, Switzerland. *Ore Geology Reviews* 95, 746-788, 2018.



- 1672 59. Kronfeld, J., Vogel, J.C. and Talma, A.S.: A new explanation for extreme $^{234}\text{U}/^{238}\text{U}$
1673 disequilibria in a dolomitic aquifer. *Earth and Planetary Science Letters*, 123, 81-93,
1674 1994.
- 1675 60. Kylander-Clark, A.R., Hacker, B.R. and Cottle, J.M.: Laser-ablation split-stream ICP
1676 petrochronology. *Chemical Geology*, 345, 99-112, 2013.
- 1677 61. Langmuir, D.: Uranium solution-mineral equilibria at low temperatures with
1678 applications to sedimentary ore deposits. *Geochimica et Cosmochimica Acta*, 42,
1679 547-569, 1978.
- 1680 62. Lawson, M., Shenton, B.J., Stolper, D.A., Eiler, J.M., Rasbury, E.T., Becker, T.P.,
1681 Phillips-Lander, C.M., Buono, A.S., Becker, S.P., Pottorf, R. and Gray, G.G.:
1682 Deciphering the diagenetic history of the El Abra Formation of eastern Mexico using
1683 reordered clumped isotope temperatures and U-Pb dating. *GSA Bulletin*, 130, 617-
1684 629, 2018.
- 1685 63. Lee, M.R., Hodson, M.E. and Langworthy, G.: Earthworms produce granules of
1686 intricately zoned calcite. *Geology*, 36, 943-946, 2008.
- 1687 64. Li, Q., Parrish, R.R., Horstwood, M.S.A. and McArthur, J.M.: U-Pb dating of cements
1688 in Mesozoic ammonites. *Chemical Geology*, 376, 76-83, 2014.
- 1689 65. Liivamägi S, Šrodon J, Bojanowski M, Gerdes A, Stanek JJ, Williams L, Szczerba
1690 M.: Paleosols on the Ediacaran basalts of the East European Craton: a unique
1691 record of paleoweathering with minimum diagenetic overprint. *Precambrian
1692 Research*, 316, 66-82, 2018.
- 1693 66. MacDonald, J.M., Faithfull, J.W., Roberts, N.M.W., Davies, A.J., Holdsworth, C.M.,
1694 Newton, M., Williamson, S., Boyce, A. and John, C.M.: Clumped-isotope
1695 palaeothermometry and LA-ICP-MS U-Pb dating of lava-pile hydrothermal calcite
1696 veins. *Contributions to Mineralogy and Petrology*, 174, 63, 2019.
- 1697 67. Machel, H.G.: Cathodoluminescence in calcite and dolomite and its chemical
1698 interpretation. *Geoscience Canada*, 12, 139-147, 1985.
- 1699 68. Machel, H.G.: Application of cathodoluminescence to carbonate diagenesis,
1700 in: *Cathodoluminescence in geosciences*, edited by Pagel M., Barbin V., Blanc P.
1701 and Ohnenstetter D., Springer, Berlin, Heidelberg, Germany, 271-301, 2000.
- 1702 69. Manganot, X., Gasparrini, M., Gerdes, A., Bonifacie, M. and Rouchon, V.: An
1703 emerging thermochronometer for carbonate-bearing rocks: $\Delta 47/(\text{U-Pb})$. *Geology*, 46,
1704 1067-1070, 2018.



- 1705 70. Maskenskaya, O.M., Drake, H., Broman, C., Hogmalm, J.K., Czuppon, G. and
1706 Åström, M.E.: Source and character of syntaxial hydrothermal calcite veins in
1707 Paleoproterozoic crystalline rocks revealed by fine-scale
1708 investigations. *Geofluids*, 14, 495-511, 2014.
- 1709 71. Mazurek, M., Davis, D.W., Madritsch, H., Rufer, D., Villa, I.M., Sutcliffe, C.N., De
1710 Haller, A. and Traber, D.: Veins in clay-rich aquitards as records of deformation and
1711 fluid-flow events in northern Switzerland. *Applied Geochemistry*, 95, 57-70, 2018.
- 1712 72. Methner, K., Mulch, A., Fiebig, J., Wacker, U., Gerdes, A., Graham, S.A. and
1713 Chamberlain, C.P.: Rapid middle Eocene temperature change in western North
1714 America. *Earth and Planetary Science Letters*, 450, 132-139, 2016.
- 1715 73. Michie, U.M. and Bowden, R.A.: UK NIREX geological investigations at
1716 Sellafield. *Proceedings of the Yorkshire Geological Society*, 50, 5-9, 1994.
- 1717 74. Milodowski, A.E., Bath, A. and Norris, S.: Palaeohydrogeology using geochemical,
1718 isotopic and mineralogical analyses: Salinity and redox evolution in a deep
1719 groundwater system through Quaternary glacial cycles. *Applied geochemistry*, 97,
1720 40-60, 2018.
- 1721 75. Milodowski, A.E., Gillespie, M.R., Naden, J., Fortey, N.J., Shepherd, T.J., Pearce,
1722 J.M. and Metcalfe, R.: The petrology and paragenesis of fracture mineralization in
1723 the Sellafield area, west Cumbria. *Proceedings of the Yorkshire Geological*
1724 *Society*, 52, 215-241, 1998.
- 1725 76. Milton, G.M. and Brown, R.M.: Adsorption of uranium from groundwater by common
1726 fracture secondary minerals. *Canadian Journal of Earth Sciences*, 24, 1321-1328,
1727 1987.
- 1728 77. Moorbath, S., Taylor, P.N., Orpen, J.L., Treloar, P. and Wilson, J.F.: First direct
1729 radiometric dating of Archaean stromatolitic limestone. *Nature*, 326, 865-867, 1987.
- 1730 78. Osmond, J.K. and Cowart, J.B.: Ground water, in: Uranium-series Disequilibrium:
1731 Applications to Earth, Marine, and Environmental Sciences, Second Edition, edited
1732 by: Ivanovich, M. and Harmon, R.S., Clarendon Press, Oxford, UK, 290-330.
- 1733 79. Osmond, J.K. and Cowart, J.B.: The theory and uses of natural uranium isotopic
1734 variations in hydrology. *Atomic Energy Review*, 14, 621-679, 1976.
- 1735 80. Osmond, J.K. and Cowart, J.B.: U-series nuclides as tracers in groundwater
1736 hydrology, in: *Environmental tracers in subsurface hydrology*, edited by Cook P.G.,
1737 and Herczeg A.L., Springer, Boston, MA, USA, 145-173, 2000.



- 1738 81. Osmond, J.K., Rydell, H.S. and Kaufman, M.I.: Uranium disequilibrium in
1739 groundwater: an isotope dilution approach in hydrologic investigations. *Science*, 162,
1740 997-999, 1968.
- 1741 82. Neymark, L.A., Holm-Denoma, C.S. and Moscati, R.J.: In situ LA-ICPMS U–Pb
1742 dating of cassiterite without a known-age matrix-matched reference material:
1743 Examples from worldwide tin deposits spanning the Proterozoic to the
1744 Tertiary. *Chemical Geology*, 483, 410-425, 2018.
- 1745 83. Nuriel, P., Craddock, J., Kylander-Clark, A.R., Uysal, T., Karabacak, V., Dirik, R.K.,
1746 Hacker, B.R. and Weinberger, R.: Reactivation history of the North Anatolian fault
1747 zone based on calcite age-strain analyses. *Geology*, 47, 465-469, 2019.
- 1748 84. Nuriel, P., Weinberger, R., Kylander-Clark, A.R.C., Hacker, B.R. and Craddock, J.P.:
1749 The onset of the Dead Sea transform based on calcite age-strain
1750 analyses. *Geology*, 45, 587-590, 2017.
- 1751 85. Palin, R.M., Searle, M.P., Waters, D.J., Parrish, R.R., Roberts, N.M.W., Horstwood,
1752 M.S.A., Yeh, M.W., Chung, S.L. and Anh, T.T.: A geochronological and petrological
1753 study of anatectic paragneiss and associated granite dykes from the Day Nui C on
1754 Voi metamorphic core complex, North Vietnam: constraints on the timing of
1755 metamorphism within the Red River shear zone. *Journal of Metamorphic
1756 Geology*, 31, 359-387, 2013.
- 1757 86. Pagel, M., Bonifacie, M., Schneider, D.A., Gautheron, C., Brigaud, B., Calmels, D.,
1758 Cros, A., Saint-Bezar, B., Landrein, P., Sutcliffe, C. and Davis, D.: Improving
1759 paleohydrological and diagenetic reconstructions in calcite veins and breccia of a
1760 sedimentary basin by combining $\Delta 47$ temperature, $\delta^{18}\text{O}_{\text{water}}$ and U-Pb age. *Chemical
1761 Geology*, 481, 1-17, 2018.
- 1762 87. Paquette, J. and Reeder, R.J.: Relationship between surface structure, growth
1763 mechanism, and trace element incorporation in calcite. *Geochimica et
1764 Cosmochimica Acta*, 59, 735-749, 1995.
- 1765 88. Parrish, R.R., Parrish, C.M. and Lasalle, S.: Vein calcite dating reveals Pyrenean
1766 orogen as cause of Paleogene deformation in southern England. *Journal of the
1767 Geological Society*, 175, 425-442, 2018.
- 1768 89. Paton, C., Hellstrom, J., Paul, B., Woodhead, J. and Hergt, J.: Lolite: Freeware for
1769 the visualisation and processing of mass spectrometric data. *Journal of Analytical
1770 Atomic Spectrometry*, 26, 2508-2518, 2011.



- 1771 90. Paton, C., Woodhead, J.D., Hellstrom, J.C., Hergt, J.M., Greig, A. and Maas, R.:
1772 Improved laser ablation U-Pb zircon geochronology through robust downhole
1773 fractionation correction. *Geochemistry, Geophysics, Geosystems*, 11, Q0AA06,
1774 DOI:10.1029/2009GC002618, 2010.
- 1775 91. Perrette, Y., Delannoy, J.J., Desmet, M., Lignier, V. and Destombes, J.L.:
1776 Speleothem organic matter content imaging. The use of a Fluorescence Index to
1777 characterise the maximum emission wavelength. *Chemical Geology*, 214, 193-208,
1778 2005.
- 1779 92. Petrus, J.A., Chew, D.M., Leybourne, M.I. and Kamber, B.S.: A new approach to
1780 laser-ablation inductively-coupled-plasma mass-spectrometry (LA-ICP-MS) using the
1781 flexible map interrogation tool 'Monocle'. *Chemical Geology*, 463, 76-93, 2017.
- 1782 93. Pevear, D.R., Vrolijk, P.J., Longstaffe, F.J., Hendry, J., Carey, P., Parnell, J., Ruffell,
1783 A. and Worden, R.: Timing of Moab fault displacement and fluid movement
1784 integrated with burial history using radiogenic and stable isotopes. *Geofluids II*, 97,
1785 42-45, 1997.
- 1786 94. Pickering, R., Kramers, J.D., Partridge, T., Kodolanyi, J. and Pettke, T.: U–Pb dating
1787 of calcite–aragonite layers in speleothems from hominin sites in South Africa by MC-
1788 ICP-MS. *Quaternary Geochronology*, 5, 544-558, 2010.
- 1789 95. Porcelli, D. and Swarzenski, P.W.: The behavior of U-and Th-series nuclides in
1790 groundwater. *Reviews in Mineralogy and Geochemistry*, 52, 317-361, 2003.
- 1791 96. Quade, J., Rasbury, E.T., Huntington, K.W., Hudson, A.M., Vonhof, H., Anchukaitis,
1792 K., Betancourt, J., Latorre, C. and Pepper, M.: Isotopic characterization of late
1793 Neogene travertine deposits at Barrancas Blancas in the eastern Atacama Desert,
1794 Chile. *Chemical Geology*, 466, 41-56, 2017.
- 1795 97. Rasbury, E.T. and Cole, J.M.: Directly dating geologic events: U-Pb dating of
1796 carbonates. *Reviews of Geophysics*, 47, 2009.
- 1797 98. Rasbury, E.T., Hanson, G.N., Meyers, W.J. and Saller, A.H.: Dating of the time of
1798 sedimentation using U-Pb ages for paleosol calcite. *Geochimica et Cosmochimica*
1799 *Acta*, 61, 1525-1529, 1997.
- 1800 99. Ray, J.S., Veizer, J. and Davis, W.J.: C, O, Sr and Pb isotope systematics of
1801 carbonate sequences of the Vindhyan Supergroup, India: age, diagenesis,
1802 correlations and implications for global events. *Precambrian Research*, 121, 103-
1803 140, 2003.



- 1804 100. Reeder, R.J.: Interaction of divalent cobalt, zinc, cadmium, and barium with
1805 the calcite surface during layer growth. *Geochimica et Cosmochimica Acta*, 60,
1806 1543-1552, 1996.
- 1807 101. Reeder, R.J., Nugent, M., Lamble, G.M., Tait, C.D. and Morris, D.E.: Uranyl
1808 incorporation into calcite and aragonite: XAFS and luminescence
1809 studies. *Environmental Science & Technology*, 34, 638-644, 2000.
- 1810 102. Reeder, R.J., Nugent, M., Tait, C.D., Morris, D.E., Heald, S.M., Beck, K.M.,
1811 Hess, W.P. and Lanzirotti, A.: Coprecipitation of uranium (VI) with calcite: XAFS,
1812 micro-XAS, and luminescence characterization. *Geochimica et Cosmochimica*
1813 *Acta*, 65, 3491-3503, 2001.
- 1814 103. Regis, D., Warren, C.J., Mottram, C.M. and Roberts, N.M.W.: Using monazite
1815 and zircon petrochronology to constrain the P–T–t evolution of the middle crust in the
1816 Bhutan Himalaya. *Journal of Metamorphic Geology*, 34, 617-639, 2016.
- 1817 104. Renne, P.R., Karner, D.B. and Ludwig, K.R.: Absolute ages aren't
1818 exactly. *Science*, 282, 1840-1841, 1998.
- 1819 105. Richards, D.A., Bottrell, S.H., Cliff, R.A., Ströhle, K. and Rowe, P.J.: U-Pb
1820 dating of a speleothem of Quaternary age. *Geochimica et Cosmochimica Acta*, 62,
1821 3683-3688, 1998.
- 1822 106. Richter, D.K., Götte, T., Götze, J. and Neuser, R.D.: Progress in application of
1823 cathodoluminescence (CL) in sedimentary petrology. *Mineralogy and Petrology*, 79,
1824 127-166, 2003.
- 1825 107. Ring, U. and Gerdes, A.: Kinematics of the Alpenrhein-Bodensee graben
1826 system in the Central Alps: Oligocene/Miocene transtension due to formation of the
1827 Western Alps arc. *Tectonics*, 35, 1367-1391, 2016.
- 1828 108. Roberts, N.M.W., Rasbury, E.T., Parrish, R.R., Smith, C.J., Horstwood,
1829 M.S.A. and Condon, D.J.: A calcite reference material for LA-ICP-MS U-Pb
1830 geochronology. *Geochemistry, Geophysics, Geosystems*, 18, 2807-2814, 2017.
- 1831 109. Roberts, N.M.W. and Walker, R.J.: U-Pb geochronology of calcite-mineralized
1832 faults: Absolute timing of rift-related fault events on the northeast Atlantic
1833 margin. *Geology*, 44, 531-534, 2016.
- 1834 110. Robertson, K., Gauvin, R. and Finch, J.: Application of charge contrast
1835 imaging in mineral characterization. *Minerals Engineering*, 18, 343-352, 2005.



- 1836 111. Russell, J., Chadwick, B., Rao, B.K. and Vasudev, V.N.: Whole-rock PbPb
1837 isotopic ages of Late Archaean limestones, Karnataka, India. *Precambrian*
1838 *Research*, 78, 261-272, 1996.
- 1839 112. Sarangi, S., Gopalan, K. and Kumar, S.: Pb–Pb age of earliest megascopic,
1840 eukaryotic alga bearing Rohtas Formation, Vindhyan Supergroup, India: implications
1841 for Precambrian atmospheric oxygen evolution. *Precambrian Research*, 132, 107-
1842 121, 2004.
- 1843 113. Savard, M.M., Veizer, J. and Hinton, R.: Cathodoluminescence at low Fe and
1844 Mn concentrations; a SIMS study of zones in natural calcites. *Journal of Sedimentary*
1845 *Research*, 65, 208-213, 1995.
- 1846 114. Scardia, G., Parenti, F., Miggins, D.P., Gerdes, A., Araujo, A.G. and Neves,
1847 W.A.: Chronologic constraints on hominin dispersal outside Africa since 2.48 Ma
1848 from the Zarqa Valley, Jordan. *Quaternary Science Reviews*, 219, 1-19, 2019.
- 1849 115. Shopov, Y.Y., Ford, D.C. and Schwarcz, H.P.: Luminescent microbanding in
1850 speleothems: high-resolution chronology and paleoclimate. *Geology*, 22, 407-410,
1851 1994.
- 1852 116. Smeraglia, L., Aldega, L., Billi, A., Carminati, E., Di Fiore, F., Gerdes, A.,
1853 Albert, R., Rossetti, F. and Vignaroli, G.: Development of an intra-wedge tectonic
1854 mélange by out-of-sequence thrusting, buttressing, and intraformational rheological
1855 contrast, Mt. Massico ridge, Apennines, Italy. *Tectonics*, 38, 1223-1249, 2019.
- 1856 117. Smith, P.E. and Farquhar, R.M.: Direct dating of Phanerozoic sediments by
1857 the ^{238}U – ^{206}Pb method. *Nature*, 341, 518, 1989.
- 1858 118. Smith, P.E., Farquhar, R.M. and Hancock, R.G.: Direct radiometric age
1859 determination of carbonate diagenesis using U–Pb in secondary calcite. *Earth and*
1860 *Planetary science letters*, 105, 474-491, 1991.
- 1861 119. Solum, J.G., van der Pluijm, B.A. and Peacor, D.R.: Neocrystallization, fabrics
1862 and age of clay minerals from an exposure of the Moab Fault, Utah. *Journal of*
1863 *Structural Geology*, 27, 1563-1576, 2005.
- 1864 120. Stacey, J.T. and Kramers, J.: Approximation of terrestrial lead isotope
1865 evolution by a two-stage model. *Earth and planetary science letters*, 26, 207-221,
1866 1975.
- 1867 121. Stübner, K., Grujic, D., Parrish, R.R., Roberts, N.M., Kronz, A., Wooden, J.
1868 and Ahmad, T.: Monazite geochronology unravels the timing of crustal thickening in
1869 NW Himalaya. *Lithos*, 210, 111-128, 2014.



- 1870 122. Sturchio, N.C., Antonio, M.R., Soderholm, L., Sutton, S.R. and Brannon, J.C.:
1871 Tetravalent uranium in calcite. *Science*, 281, 971-973, 1998.
- 1872 123. Suksi, J., Rasilainen, K. and Pitkänen, P.: Variations in $^{234}\text{U}/^{238}\text{U}$ activity
1873 ratios in groundwater—A key to flow system characterisation?. *Physics and*
1874 *Chemistry of the Earth, Parts A/B/C*, 31, 556-571, 2006.
- 1875 124. Sumner, D.Y. and Bowring, S.A.: U-Pb geochronologic constraints on
1876 deposition of the Campbellrand Subgroup, Transvaal Supergroup, South
1877 Africa. *Precambrian Research*, 79, 25-35, 1996.
- 1878 125. Taylor, P.N. and Kalsbeek, F.: Dating the metamorphism of Precambrian
1879 marbles: Examples from Proterozoic mobile belts in Greenland. *Chemical Geology:*
1880 *Isotope Geoscience Section*, 86, 21-28, 1990.
- 1881 126. Trudgill, B.D.: Evolution of salt structures in the northern Paradox Basin:
1882 Controls on evaporite deposition, salt wall growth and supra-salt stratigraphic
1883 architecture. *Basin Research*, 23, 208-238, 2011.
- 1884 127. Tullborg, E.L., Drake, H. and Sandström, B.: Palaeohydrogeology: a
1885 methodology based on fracture mineral studies. *Applied Geochemistry*, 23, 1881-
1886 1897, 2008.
- 1887 128. Ukar, E. and Laubach, S.E.: Syn- and postkinematic cement textures in
1888 fractured carbonate rocks: Insights from advanced cathodoluminescence
1889 imaging. *Tectonophysics*, 690, 190-205, 2016.
- 1890 129. Uysal, I.T., Feng, Y.X., Zhao, J.X., Bolhar, R., Işık, V., Baublys, K.A., Yago, A.
1891 and Golding, S.D.: Seismic cycles recorded in late Quaternary calcite veins:
1892 geochronological, geochemical and microstructural evidence. *Earth and Planetary*
1893 *Science Letters*, 303, 84-96, 2011.
- 1894 130. Walter, B.F., Gerdes, A., Kleinhanns, I.C., Dunkl, I., von Eynatten, H., Kreisss,
1895 S. and Markl, G.: The connection between hydrothermal fluids, mineralization,
1896 tectonics and magmatism in a continental rift setting: Fluorite Sm-Nd and hematite
1897 and carbonates U-Pb geochronology from the Rhinegraben in SW
1898 Germany. *Geochimica et Cosmochimica Acta*, 240, 11-42, 2018.
- 1899 131. Warren, C.J., Singh, A.K., Roberts, N.M.W., Regis, D., Halton, A.M. and
1900 Singh, R.B.: Timing and conditions of peak metamorphism and cooling across the
1901 Zimithang Thrust, Arunachal Pradesh, India. *Lithos*, 200, 94-110, 2014.



- 1902 132. Watt, G.R., Griffin, B.J. and Kinny, P.D.: Charge contrast imaging of
1903 geological materials in the environmental scanning electron microscope. *American*
1904 *Mineralogist*, 85, 1784-1794, 2000.
- 1905 133. Weremeichik, J.M., Gabitov, R.I., Thien, B.M. and Sadekov, A.: The effect of
1906 growth rate on uranium partitioning between individual calcite crystals and
1907 fluid. *Chemical Geology*, 450, 145-153, 2017.
- 1908 134. Wendt, I. and Carl, C.: The statistical distribution of the mean squared
1909 weighted deviation. *Chemical Geology: Isotope Geoscience Section*, 86, 275-285,
1910 1991.
- 1911 135. Whitehouse, M.J. and Russell, J.: Isotope systematics of Precambrian
1912 marbles from the Lewisian complex of northwest Scotland: implications for Pb–Pb
1913 dating of metamorphosed carbonates. *Chemical Geology*, 136, 295-307, 1997.
- 1914 136. Williams, R.T., Goodwin, L.B., Sharp, W.D. and Mozley, P.S.: Reading a
1915 400,000-year record of earthquake frequency for an intraplate fault. *Proceedings of*
1916 *the National Academy of Sciences*, 114, 4893-4898, 2017.
- 1917 137. Woodhead, J., Hellstrom, J., Maas, R., Drysdale, R., Zanchetta, G., Devine,
1918 P. and Taylor, E.: U–Pb geochronology of speleothems by MC-ICPMS. *Quaternary*
1919 *Geochronology*, 1, 208-221, 2006.
- 1920 138. Woodhead, J., Hellstrom, J., Pickering, R., Drysdale, R., Paul, B. and Bajo,
1921 P.: U and Pb variability in older speleothems and strategies for their
1922 chronology. *Quaternary Geochronology*, 14, 105-113, 2012.
- 1923 139. Woodhead, J.D., Sniderman, J.K., Hellstrom, J., Drysdale, R.N., Maas, R.,
1924 White, N., White, S. and Devine, P.: The antiquity of Nullarbor speleothems and
1925 implications for karst palaeoclimate archives. *Scientific reports*, 9, 603, 2019.
- 1926 140. Yokoyama, T., Kimura, J.I., Mitsuguchi, T., Danhara, T., Hirata, T., Sakata, S.,
1927 Iwano, H., Maruyama, S., Chang, Q., Miyazaki, T. and Murakami, H.: U-Pb dating of
1928 calcite using LA-ICP-MS: Instrumental setup for non-matrix-matched age dating and
1929 determination of analytical areas using elemental imaging. *Geochemical Journal*, 52,
1930 531-540, 2018.